

Published in final edited form as:

Science. 2024 September 20; 385(6715): eadd8947. doi:10.1126/science.add8947.

Germline mutations in a G-protein identify signaling crosstalk in T cells

A full list of authors and affiliations appears at the end of the article.

Abstract

*Corresponding author. hsu@niaid.nih.gov.

Author contributions:

H.H. identified the interaction between active Gai2 and RASA2, performed experiments examining TCR-induced responsiveness of mutant Gai2 transduced T cells, TCR-induced signaling of patient T cells, transduced T cells, and RASA2-depleted T cells, validated GNAI2 mutant allele (P1)-specific KO, and performed GST-pulldowns, communoprecipitations, GAP assays, confocal microscopy, FLIM imaging, in vitro chemotaxis, and GTPase assays. H.J. performed experiments evaluating Gai2 variants by cAMP ELISA or reporter BRET assay and in vitro transwell chemotaxis, TCR-induced responsiveness of patient and KO T cells (GNAI2 mutant allele (P1), RASA2, and ACs), and TCR-induced signaling of AC-KO T cells. I.T.L. identified and established the causal nature of patient GNAI2 mutations, made initial observation of impaired chemotaxis, Ca²⁺ flux, and TCR-induced hyperresponsiveness, as well as performed experiments examining proximal and downstream signaling, in vitro transwell chemotaxis, chemokine induced Ca^{2+} flux, and $G_{\alpha i2}$ expression in patient and mutant $G_{\alpha i2}$ transduced T cells. I.T.L., J.N.M., R.N.G. studied chemotaxis in vivo using adoptive cell transfer. M.M.K. performed TCR-induced activation and signaling experiments of patient T cells. A.K., V.L.K. performed GTP binding and GTP hydrolysis by Gai variants and analyzed data. Y.A.B., T.P.S. set up BRET assay to evaluate $G_{\alpha,i,2}$ mutant from P1 and examine the interaction of $G_{\alpha,i,2}$ and GPCR. D.E.A. performed mass spectrometry analysis to identify interacting proteins. K.M.D. performed RGS protein pull-down. M.K., S.R. performed cAMP measurements of Gai2 variants using Glo-sensor. D.B.K., D.L.F., X.X, W.S.K., T.J. performed EZ-TAXIScan experiments. K.A.Z. evaluated leukocyte migration into blisters. N.M.M. evaluated cell accumulation in oral mucosa. H.H.K. performed skin virome analysis. P.C. performed molecular modeling. M.M.K., J.D., and D.T. assisted in $G_{\alpha i2}$ expression, in vitro chemotaxis, GTPase assay, and processing patient samples. Ka.Me. performed coimmunoprecipitation of exogenously expressed RASA2 with G_{G12} variants. M.F.R.Q. assisted with TCR-induced signaling experiments of patient T cells. S.G. and J.K. assisted with imaging capture and analyses. E.M.-F., R.B., C.C.G. generated and evaluated the Gnai2 KI mice. V.J.W, generated the AC3 and AC6 double KO HEK293 cells and advised on cAMP assays. D.D.B. assisted in analyses of data for manuscript preparation.

Experimental patient biospecimens and clinical data were collected/curated by P.J.M., H.C.S., J.T., B.I., A.F.F., Z.Z.-C., C.K., L.F., P.E., W.A.-H., J.P.S., K.V., P.A.T., V.B., L.P., M.M., P.L., K.N.O., A.N., M.L.-N., B.M., O.M.M., F.H., P.S., Me.Wo., K.E.S., Ma.Sl., Ma.So., H.H.K., Sé.Ba., H.S., R.J., D.L. Genetic studies (WES/WGS, Ion Torrent panel, Sanger confirmation) were performed, analyzed, or coordinated by Y.Z., S.K., C.S., R.J.T., N.C., C.K., F.L., Ma.Wa., R.P., M.M., A.P., Ja.Ch., G.L., A.-L.B., M.T., P.L., T.B., J.D., G.T., Y.D., A.P.H., J.S., S.L., Mo.Si., J.-L.C., O.M.M., Jo.Ch., St. Bé., R.S.G., C.A.S., H.S., B.K., B.B.-P., P.B., Ki.Mc. Across the patient cohort, dysmorphism and skeletal imaging were evaluated and analyzed by C.R.F., neurological imaging was analyzed by A.S., and S.P. performed histopathologic analyses. A.F.F. and I.T.L. assisted H.C.S. in overall clinical data curation. A.J.O. performed categorical analyses of HPO data. J.G. assisted with statistical analyses.

H.F.M. coordinated clinical study protocol and sample collection. H.C.S. planned and supervised the experimental work and data analyses. M.J.L. provided advice and assisted in supervising experimental work. Y.Z. performed, supervised, and coordinated genetic studies including Sanger sequencing mutation confirmations, WES re-analysis across the cohort and RNA-seq analyses. H.H., H.J., I.T.L., M.J.L., and H.C.S. prepared the manuscript. All authors read and discussed the submitted manuscript.

Competing interests: H.C.S. holds stock in Amgen and Eli Lilly. K.M. is an employee of GeneDx, a genetic testing laboratory. R.J.T. is an Illumina Inc employee and shareholder. J.P.S. was a member of a data monitoring committee for Leniolisib for SOBI and Pharming within the last 3 years. C.A.S. was a paid consultant for Lundbeck pharmaceuticals. C.A.S. is an inventor on patent applications US-20030022180-A1 held by NIH that covers PRKAR1A and Carney complex, US-20090005337-A1 held by NIH that covers PDE11A and adrenal disease, US-20170304405-A1 held by NIH that covers treatment of hormonal disorders of growth, and US-20190314459-A1 held by NIH that covers GPR101 function. The other authors declare that they have no competing interests.

Present address

Present address: Department of Physiology, McGill University; Montreal, QC Canada.

^{*}Present address: Blanchard Valley Hospital; Findlay, OH, USA.

^{**}Present address: Department of Biomedical Sciences, Humanitas University, Milan, Italy. IRCCS Humanitas Research Hospital; Milan, Italy.

^{††}Present address: ELPEN, Inc, Pikermi, Athens, Greece. HUMAN LONGEVITY, San Diego, CA, USA. STEROTHERAPEUTICS, Doylestown, PA, USA

These authors contributed equally to this work.

These authors contributed equally to this work.

^{‡‡}These authors contributed equally to this work

Humans with monogenic inborn errors responsible for extreme disease phenotypes can reveal essential physiological pathways. We investigated germline mutations in GNAI2, which encodes $G_{\alpha i2}$, a key component in heterotrimeric G-protein signal transduction usually thought to regulate adenylyl cyclase-mediated cAMP production. Patients with activating $G_{\alpha i2}$ mutations had clinical presentations that included impaired immunity. Mutant $G_{\alpha i2}$ impaired cell migration and augmented responses to T cell receptor (TCR) stimulation. We found that mutant $G_{\alpha i2}$ influenced TCR signaling by sequestering the GTPase-activating protein RASA2, thereby promoting RAS activation and increasing downstream ERK/MAPK and PI3K-AKT S6 signaling to drive cellular growth and proliferation.

One-Sentence Summary:

Activating $G_{\alpha i2}$ mutations in a syndromic disorder reveal a cAMP-independent, $G_{\alpha i2}$ -RASA2-RAS pathway regulating T cell responsiveness.

Introduction

G-protein coupled receptors (GPCRs) are fundamental to mammalian physiology (1, 2). They direct cells to respond to diverse environmental cues including hormones, neurotransmitters, and chemokines. This is accomplished through a complex and highly regulated biochemical cycle mediated by associated heterotrimeric G-proteins ($G_{\alpha\beta\gamma}$). After GPCR ligation, the G_{α} subunit binds GTP, becomes active, and dissociates from both the $G_{\beta\gamma}$ complex and the GPCR. Dissociation causes both G_{α} -GTP and free $G_{\beta\gamma}$ to initiate downstream signals including generation of second messengers and ion fluxes. Ultimately, the GTPase activity of G_{α} hydrolyzes GTP into GDP to terminate signaling and allow reassembly of the heterotrimeric G-protein that can reassociate with a GPCR, completing the cycle and resetting cells to allow them to respond again to GPCR engagement (3).

The 16 human G_{α} subunits are grouped into four families ($G_{\alpha s}$, $G_{\alpha i/o}$, $G_{\alpha q/11}$, and $G_{\alpha 12/13}$) having distinct expression patterns and effector partners (4). The $G_{\alpha i/o}$ family includes inhibitory isoforms of G_{α} that are thought to regulate biological responses by suppressing adenylyl cyclase (AC) production of the intracellular second messenger, cyclic AMP (cAMP) (5). AC exist as nine transmembrane isoforms expressed broadly, with different tissues expressing different levels of multiple isoforms (6, 7). Only group III (AC5, AC6) and to a lesser degree group I (AC1) ACs are sensitive to the inhibitory effects of $G_{\alpha i}$ (6, 7).

Humans with monogenic inborn errors responsible for extreme disease phenotypes can reveal essential physiological pathways. Germline mutations in $G_{\alpha i/o}$ family members (*GNAI1*, *GNAI3*, *GNAO1*, *GNAT1*, *GNAT2*) cause severe neurodevelopmental, craniofacial, or visual system defects (8–10). By contrast, the effect of germline *GNAI2* mutations in humans is not known. While $G_{\alpha i2}$ (encoded by *GNAI2*) is ubiquitously expressed, it has been implicated in normal functioning of the cardiovascular, nervous, endocrine, and immune systems (11, 12). Somatic *GNAI2* mutations that activate $G_{\alpha i2}$ have been identified in human ovarian and adrenal tumors (13). *GNAI2* variants of unknown significance were also identified in two individuals with neurodevelopmental defects (14, 15).

Since the roles of $G_{\alpha i2}$ in human physiology and development are not clear, we sought to identify individuals that harbor mutations in *GNAI2* to examine their clinical presentations and their underlying disease mechanisms.

GNAI2 mutations found in humans inhibited the intrinsic GTPase activity

We used whole exome/genome sequencing to discover 20 patients from 18 unrelated families of different ancestries worldwide, who had previously unreported or extremely rare heterozygous missense variants in GNAI2, which were also computationally predicted to be deleterious (CADD score > 25) (Fig. 1A, and table S1). The variants were absent in the Greater Middle Eastern Variome (16) and in the Genome Aggregation Database (gnomAD v3.1.2) (17), except for 3–50256263-G-A (GRCh38, p.Arg179His), which was found in 1 individual (minor allele frequency (MAF) 0.00002494 in the African/African American population) of unknown affectation status. In our families, the variants segregated with a hitherto unrecognized autosomal dominant syndromic disorder, in which $de\ novo\ (N=12)$ mutations predominated. These mutations were detected in several tissues (fig. S1, A and B), suggesting they arose in germ cells or early during embryonic development. The patients' cells expressed equivalent levels of both mutant and wild-type (WT) transcripts, as well as normal levels of total $G_{\alpha i2}$ protein (fig. S1, C and D).

The mutations caused amino acid substitutions at residues that were evolutionarily constrained and highly conserved in all heterotrimeric G-protein superfamily members (Fig. 1B and fig. S1E). The altered residues were clustered in the Ras-like GTPase domain of G_{α} , especially within the highly conserved P-loop motif and switch regions that are critical for guanine-nucleotide binding and GTPase activity (Fig. 1B and fig. S1E). These mutations could interfere with binding of the GTP phosphate group and cofactors (Mg^{2+} ion, nucleophilic H_2O) that are necessary to hydrolyze bound GTP (Fig. 1 C) or could indirectly influence GTP binding/hydrolysis (fig. S2, A to C), which would likely result in impaired signal termination (see Supplementary Text 1).

We tested the function of purified recombinant $G_{\alpha i2}$ variant proteins and compared their ability to bind and hydrolyze GTP with non-mutated WT $G_{\alpha i2}$ and a GTPase-mutant (Gln205Leu) known to be deficient in GTP hydrolysis (18). In general, the $G_{\alpha i2}$ mutants, except Arg179His, bound non-hydrolyzable GTP $_{\gamma}$ S more readily than WT (Fig. 1, D and E; fig. S2, D to F; and table S2) and all exhibited decreased GTP hydrolysis (Fig. 1, F and G; fig. S2, G to J; and table S2).

To substantiate the conclusion that the mutations in $G_{\alpha i2}$ impaired GTPase activity, we investigated their regulation by regulators of G-protein signaling (RGS). The intrinsic GTPase activity of $G_{\alpha i}$ is normally accelerated by RGS which act as GTPase activating proteins (GAPs) and are strictly dependent on binding to a G_{α} transition state conformation (18). GTPase-deficient G_{α} mutants, such as $G_{\alpha i1}$ -Gln204Leu, are generally resistant to RGS GAP activity (19). Accordingly, the GTPase activities of the patients' $G_{\alpha i2}$ mutants, except Arg179His, were not increased by adding RGS16 (Fig. 1G and fig. S2J). Furthermore, neither of two patient mutants we tested (Thr182Ala/Ile, nor Gln205Leu) bound RGS16 (fig. S2, K and L), similar to an RGS-insensitive Gly184Ser control (20). Taken together,

the faster GTP binding, decreased GTPase activity, and RGS insensitivity indicated that the patients' $G_{\alpha i2}$ mutant proteins could promote a GTP-bound form of $G_{\alpha i2}$, in this way delaying signal termination and prolonging $G_{\alpha i2}$ activity (table S2).

This constitutive activation of $G_{\alpha i2}$ would be expected to overstimulate downstream functions such as inhibition of cAMP production (5). Therefore, we measured forskolin (FSK)-induced AC synthesis of cAMP in the presence of overexpressed $G_{\alpha i2}$. Compared to WT, mutant $G_{\alpha i2}$ found in patients suppressed accumulated cAMP production (Fig. 1H, and fig. S3, A to D) or transient cAMP activity (Fig. 1I; fig. S3, E to H; and table S3). AC5 is a well-documented target of active $G_{\alpha i2}$ inhibition (5), and we observed similar effects of mutant $G_{\alpha i2}$ on AC5-induced cAMP production (fig. S3D). Finally, primary dermal fibroblasts isolated from several patients (bearing Thr182Ala, Lys46Thr, Arg209Trp mutations) showed decreased cAMP production (Fig. 1J). However, two mutants tested, including Arg209Trp, did not decrease cAMP production in the overexpression system (Fig 1H and table S2). Mutations at Arg209, which is part of a highly conserved "Gly-Arg-Glu" triad found in all G_{α} family members, can disable G_{α} activation of effectors due its inability to dissociate from $G_{\beta\gamma}$ even in the GTP-bound conformation (Supplementary Text 2) (21).

Overall, our data suggested that the mutations in GNAI2 that we identified in patients impaired the GTPase activity of $G_{\alpha i2}$ and enhanced the suppression of cAMP production, which would be consistent with them being pathogenic "activating" variants.

Patients with GNAI2 mutations exhibited multiple clinical presentations

We next investigated the overall pathophysiological impact of the activating $G_{\alpha i2}$ mutations by in-depth clinical phenotyping (Data File S1 and Supplementary Text 3 and 4). The patients exhibited abnormal development characterized by intrauterine growth retardation, dysmorphism (Fig. 2A), bone dysostosis (Fig. 2B), neuroanatomical abnormalities (Fig. 2C), and birth defects in other organs (Fig. 2D). Midline structural defects, located along the body's central vertical axis and suggestive of abnormal development during blastogenesis, were observed (fig. S4A). These were most commonly congenital nasal septum deviation (Fig. 2B), dysgenesis of the corpus callosum (Fig. 2C), pituitary hypoplasia with growth hormone deficiency (Fig. 2C), Chiari I malformation (Fig. 2C), micropenis, sagittal cleft ("butterfly") vertebrae (Fig. 2B), and scoliosis (Fig. 2B). The occurrence of certain rare birth defects, such as subcortical band heterotopia (Fig. 2C), agenesis of olfactory bulbs (Fig. 2C), and coloboma, suggested defective neuronal migration during late embryogenesis/ early fetal development, including that of olfactory and gonadotropin-releasing hormone neurons as well as retinal progenitor cells. Most patients exhibited postnatal abnormalities too, including short stature with neurodevelopmental delay, neurobehavioral deficits, and gastrointestinal dysfunction (Data File S1, and Supplementary Text 3 and 4).

Weighted analysis of clinical features affected in each patient revealed heterogeneity in the systems affected across the cohort (Fig. 2E). Nearly all patients (90%) had disease involvement in the immune system, characterized by recurrent, unusual, and/or severe infections (Data File S1 and Supplementary Text 3). However, the extent of disease involvement in the immune system was greater in patients mutated at residue Thr182 due

to their additional inflammatory or autoimmune complications (Fig. 2E). An attempt to knock-in (KI) the highly constitutively activating Thr182Ile mutation into mice failed to generate heterozygous embryos beyond the eight-cell stage, indicating *in utero* lethality (table S4).

Among the immune system presentations (Data File S1 and Supplementary Text 3), bacterial, superficial fungal, or unusually severe viral infections of the skin were striking, and included recurrent shingles, extensive warts, and rubella vaccine-associated skin granulomas (Fig. 2D and fig. S4, B and C). Respiratory, middle ear, and sinus infections were common with some developing bronchiectasis, and some had invasive bacterial infections (Fig. 2B and D; and fig. S4, B and C). Inflammatory or autoimmune complications included lymphocytic infiltration of organs, psoriasis, discoid lupus, autoimmune cytopenias with splenomegaly, Hashimoto thyroiditis, type I diabetes mellitus, colitis, or macrophage activation syndrome (Fig. 2D and fig. S4). Several had asthma or atopic dermatitis (fig. S4). Longitudinal laboratory testing revealed monocytosis and neutrophilia precipitated by acute infection, which persisted in some patients (fig. S5A, and Supplementary Text 5). T cell counts were initially low, with decreased recent thymic emigrants and paucity of naïve versus effector/memory T cells, but counts increased with age (fig. S5, B to D). Effector phenotype T cells showed cytokine perturbations including increased IL-17 expression (fig. S5E). Lymphocyte proliferation and activation appeared normal or even increased (fig. S6, and table S5). Dysgammaglobulinemia, characterized by low serum IgM and poorer vaccine titers, was accompanied by decreased B cell counts and atretic lymphoid follicles in secondary lymphoid organs (fig. S5, F and G; fig. S7; table S6; and Supplementary Text 6).

Overall, the patients' phenotypes indicated that mutant $G_{\alpha i2}$ caused multi-organ dysfunction, including life-threatening immunodysregulation and numerous birth defects. Their presentations underscore the importance of $G_{\alpha i2}$ in regulating diverse physiologic processes in humans.

G_{ai2} mutant proteins impaired immune cell migration

The patients' clinical features suggested impaired migratory behavior of immune cells for host defense, which are guided to sites of infection by chemokine receptors. Since heterotrimeric G-proteins transduce signals for all chemokine receptors (22), we tested whether hyperactive $G_{\alpha i2}$ altered cell migration. Both CD4⁺ and CD8⁺ T cells from several patients showed decreased chemotaxis toward multiple chemokines (Fig. 3A, and fig. S8, A to D) and reduced chemokine-induced Ca^{2+} fluxes mediated by free $G_{\beta\gamma}$ subunits in one tested patient (Fig. 3B, and fig. S8E), indicating defective proximal GPCR signaling. These defects were recapitulated by expressing all hyperactive $G_{\alpha i2}$ mutant proteins except Ile55Met in T cells from normal healthy donors, with intermediate and more variable effects of Leu38Arg and Arg179Cys (Fig. 3, C to E, fig. S8, F to H, and S9, A to E). Neutrophils from several patients also showed reduced directional migration in response to chemoattractants (fig. S10, A and B), and their defective migration was recapitulated by expressing several hyperactive $G_{\alpha i2}$ mutant proteins in the neutrophil-like HL60 cell line (fig. S10, C to F, and Movie S1–3). These data would be consistent with immune

cells having altered trafficking in patients with *GNAI2* mutations. Indeed, in one patient with periodontitis, leukocytes had impaired accumulation in the oral mucosa, or impaired migration into blisters after induction of sterile inflammation in the skin (fig. S10, G and H).

Furthermore, in two patients, splenic biopsies showed increased leukocyte numbers in red pulp with decreased white pulp (fig. S7 and Supplementary Text 6), suggesting that leukocyte migration into secondary lymphoid organs was also impaired. Hence, we tracked T cell migration in mice after adoptive transfer and found that cells expressing mutant $G_{\alpha i2}$ proteins migrated less well into lymph nodes and splenic white pulp (Fig. 3F, and fig. S9F). This might alter cell-cell interactions that normally take place within secondary lymphoid organs for developing immune cell functions.

Lastly, while suppressed cAMP could contribute to the impaired migration phenotype, the literature is contradictory (23). At least in T cells and neutrophils, pharmacologic manipulations that increase intracellular cAMP have been shown to inhibit chemotaxis (24, 25). Thus, we examined whether cAMP levels affected by Gai2 mutants impact T cell chemotaxis. We used CRISPR-Cas9-mediated gene editing to knockout (KO) ADCYs encoding major ACs expressed in human T cells (fig. S11, A and B). Ablation of AC3 or AC7 in healthy donor T cells had opposite effects on endogenous cAMP levels but did not affect chemotaxis, which instead segregated with the absence or presence of the mutant $G_{\alpha i2}$ (Fig. 3, G to I, and fig. S11, C to G). These results suggested that the impaired leukocyte chemotaxis in the patients did not result from $G_{\alpha i2}$ -mediated alterations in cAMP production.

Collectively, these findings showed that the patients' $G_{\alpha i2}$ mutants caused defective cell migration. We hypothesized that the patients' mutants, being in a "quasi-permanent" GTP-bound state of biochemical activation, might be mostly dissociated from GPCRs and therefore unable to transduce GPCR signals.

Using bioluminescence resonance energy transfer (BRET) to measure the interaction of $G_{\alpha i2}$ proteins with GPCRs overexpressed in living cells, we found that the Thr182Ala $G_{\alpha i2}$ mutant found in patients and Gln205Leu activating mutant control protein showed minimal steady state interaction with chemokine receptors (Fig. 3, J and K, and fig. S12, A to C). Even with ligand engagement across a broad range of concentrations, the already low BRET intensity remained unchanged, in contrast to the high BRET signal that rapidly declined to similarly low levels in cells overexpressing WT $G_{\alpha i2}$ (Fig. 3K, and fig. S12A). Increased dissociation from GPCRs also compromised chemokine-augmented suppression of transient cAMP production for several other patients' mutants (fig. S12, D and E). Hence, more potent "active" mutant $G_{\alpha i2}$ constitutively adopted a conformation that promoted decoupling from GPCRs, decreasing the pool of GPCR-WT $G_{\alpha i2}$ complexes able to recycle to active receptor complexes that can transduce GPCR signals for further biological responses.

Taken together, activating mutant $G_{\alpha i2}$ proteins had the seemingly paradoxical effect of impairing responsiveness to chemokines/chemoattractants because the mutant $G_{\alpha i2}$ proteins associate poorly to the receptors. This resulting impaired migration of immune cells can explain the patients' increased infection susceptibility.

T cells from patients with mutant $G_{\alpha i2}$ proteins were hyperresponsive to TCR stimulation

While impaired leukocyte migration could explain the patients' infection susceptibility, some patients also had life-threatening autoimmunity. Patients did not show decreased peripheral blood T_{reg} or increased CD21^{lo} CD38^{lo} B cell numbers that could account for their autoimmunity (fig. S5, D and F). However, we noticed that overall lymphocyte proliferative responses to mitogens and antigens were not decreased but appeared normal or even higher than expected (fig. S6 and Supplementary Text 5).

We hypothesized that T cell hyperresponsiveness might explain the autoimmunity in patients. Therefore, we examined T cell behavior in vitro under various T cell receptor (TCR)-stimulating conditions. Similar to our observations for gated T cells stimulated in peripheral blood mononuclear (PBMC) preparations (fig. S6), T cells purified from multiple patients (whether CD4⁺ or CD8⁺ T cells, or naïve or effector/memory T cells) exhibited enhanced induction of the activation markers CD69 and CD25 (interleukin-2 (IL-2) receptor α subunit) and increased proliferation upon stimulation with anti-CD3 plus anti-CD28 antibodies compared to control samples (Fig. 4, A to F, and fig. S13, A to L). These differential responses were also seen when cells were stimulated suboptimally (anti-CD3 antibodies only) but were not apparent when cells were treated with more potent stimulation (Beads, consisting of immobilized anti-CD2, anti-CD3, and anti-CD28 antibodies). The presence of exogenously provided IL-2 throughout the experiments and normal IL-2 production by ex vivo CD4⁺ T cells (fig. S5E) suggested that the increased responses of the patient T cells did not result from increased IL-2 production.

To determine whether the increased T cell responsiveness was a direct effect of the mutant $G_{\alpha i2}$ protein, we designed a guide RNA sequence (named gMP) that specifically knocks out the mutant but not WT *GNAI2* allele of P1 using a CRISPR-Cas9 ribonucleoprotein system (fig. S14, A to C). Treatment with gMP restored activation and proliferation of patient T cells to normal levels indicating a positive role for the mutant protein in the increased T cell responsiveness (Fig. 4, G to I and fig. S14, D and E). Transduction of CD4⁺ T cells from healthy normal donors with the Thr182Ala or Gln205Leu activating $G_{\alpha i2}$ mutants also increased TCR-induced responsiveness similar to patient T cells (Fig. 4, J and K, and fig. S13, M to Q), whereas partial KO of $G_{\alpha i2}$ in T cells from healthy donors failed to do so (fig. S14, F to H). Thus, activating- but not WT- $G_{\alpha i2}$ protein increased the stimulatory response to TCR engagement.

Proteins involved in TCR signaling showed increased distal phosphorylation in cells with mutant $G_{\alpha i2}$

T cell activation through the TCR initiates multiple signals that lead to rapid clonal expansion including activation of the RAS proteins (HRAS, KRAS, NRAS) facilitated by RAS guanyl-releasing proteins (RASGRPs) (26, 27). Activation of these small G-proteins in turn leads to activation of the extracellular signal-regulated kinase (ERK)/mitogen-activated protein kinase (MAPK) pathway, in parallel with the phosphatidylinositol

3-kinase (PI3K)-AKT-mechanistic target of rapamycin (mTOR) pathway (26, 27). Together, these signaling pathways promote a metabolic shift to aerobic glycolysis and an increase in protein synthesis for optimal cellular growth, proliferation, and differentiation. By contrast, overstimulation of these pathways can contribute to uncontrolled growth as seen in cancers, which have a high prevalence of somatic mutations in RAS, as well as certain leukoproliferative disorders associated with autoimmunity (28). G_{α} proteins are canonically thought to function by modulating production of the second messenger cAMP (2). They mediate GPCR signaling mainly at the inner leaflet of the plasma membrane (PM) and may themselves be regulated during TCR activation (29, 30). Therefore, we examined how the mutant activating $G_{\alpha i2}$ protein influences early events mediated by the TCR signaling complex at the PM. Previous work has shown that local cAMP at the PM of T cells stimulates the PKA-CSK pathway, which can counteract TCR signaling by deactivating the LCK non-receptor tyrosine kinase (29–31).

We found that both freshly isolated and previously activated patient T cells showed normal, not increased, TCR proximal signaling (Fig. 5, A to D; fig. S15, A to D, and I to L; and fig. S16, A to D). However, the same cells showed enhanced distal phosphorylation of ribosomal S6 protein, a hallmark of growth and proliferation (Fig. 5, E to G; fig. S15, E, F, M, and N; and fig. S16, E and H to J). S6 phosphorylation is mainly regulated by ERK/MAPK and PI3K-AKT signaling pathways (Fig. 5G, right) (32). Indeed, we observed enhanced and prolonged phosphorylation of ERK1/2 and p90RSK as well as AKT and p70S6K, in patient T cells and in healthy donor CD4+ T cells transduced to express activating mutant $G_{\alpha i2}$ proteins (Fig. 5, G to L; fig. S15, G, H, O, and P; and fig. S16, F to J). Treating patient T cells with the PI3K/AKT/mTOR pathway inhibitor LY294002 and the mitogen-activated or extracellular signal—regulated protein kinase kinase (MEK) inhibitor U0126 normalized S6 phosphorylation by preventing hyperactivation of AKT and p90RSK, respectively (fig. S17). Thus, active $G_{\alpha i2}$ protein augments TCR-induced ERK/MAPK and PI3K/AKT/mTORC1 signaling pathways at a step unexpectedly downstream of proximal TCR signaling events.

Mutant $G_{\alpha i2}$ modulated TCR-dependent signaling independently of cAMP

We determined that mutant $G_{\alpha i2}$ proteins from the patients inhibited AC-mediated cAMP production and that patient fibroblasts produced less cAMP (Fig. 1, H to J, and fig. S3). However, intracellular cAMP, when raised, generally plays suppressive roles in immune cells (30). Therefore, suppression of cAMP production by mutant $G_{\alpha i2}$ proteins might cause increased T cell responsiveness. We found that patient T cells produced cAMP at levels within the range of healthy donor T cells (Fig. 6A). This would be consistent with the major ACs expressed in primary human T cells being AC3, AC7, and AC9 (fig. S11, A and B), and which are not expected to show substantial regulation by $G_{\alpha i2}$ (6, 7).

To investigate the role of cAMP in T cell hyperresponsiveness further, we investigated whether manipulating cAMP levels could mimic or rescue the patient T cell phenotypes. KO of AC3 or AC7 in healthy donor T cells had elevated or decreased endogenous cAMP levels respectively, but neither affected TCR-induced S6-regulatory signaling, cellular activation, or proliferation (Fig. 6, B to F; fig. S11, C and D; and fig. S18). Furthermore, an exogenously added cAMP analog failed to normalize the increased responsiveness of patient

T cells (fig. S19). Although these approaches did not specifically measure or manipulate local cAMP levels near the PM microdomain, the normal TCR proximal signaling in patient T cells suggests $G_{\alpha i2}$ may not affect local cAMP pools (Fig. 5, A to D; fig. S15, A to D and I to L; and fig. S16, A to D).

Thus, our findings would be consistent with $G_{\alpha i2}$ proteins regulating TCR signaling via cAMP-independent mechanisms.

The interaction between $G_{\alpha i2}$ and RASA2 regulated TCR-dependent responses

To determine how hyperactive $G_{\alpha i2}$ protein may regulate S6-regulatory signaling pathways through cAMP-independent mechanisms, we investigated $G_{\alpha i2}$ -interacting proteins by performing affinity pulldown followed by quantitative mass-spectrometry. For these experiments, we used $G_{\alpha i2}$ -Thr182Ala bound to GTP $_{\gamma}$ S as the bait protein, reasoning that relevant interactors might preferentially bind the active form of $G_{\alpha i2}$. We identified well-known and previously reported interactors of $G_{\alpha i2}$ (e.g., G_{β} subunits, RGS, G-protein signaling modulator proteins, RASA3), and previously unappreciated interacting proteins (including RASA2, PP2A-A α , PP2A-C α) (Fig. 6G and Data File S2). We did not detect any AC in our $G_{\alpha i2}$ -interacting proteins, which would support that the T cell hyperresponsive phenotype may be regulated by cAMP-independent mechanisms.

RASA2, a member of the RasGAP (Ras GTPase-activating protein) family, was an intriguing candidate because its target, the RAS proteins, are major upstream regulators for the ERK/MAPK and PI3K pathways (33, 34) that were augmented in the patients' T cells (Fig. 5). We confirmed the $G_{\alpha i2}$ -RASA2 interaction by coimmunoprecipitations from lysates of cells overexpressing RASA2 and $G_{\alpha i2}$ proteins (Fig. 6H), or of endogenously expressed proteins in patient T cells (Fig. 6I). Interactions of RASA2 with multiple different activating mutant $G_{\alpha i2}$ proteins were stronger than with WT $G_{\alpha i2}$, suggesting that RASA2 might be an effector target of $G_{\alpha i2}$ (Fig. 6, H and I, and fig. S20A). Purified WT $G_{\alpha i2}$ protein directly bound RASA2 when loaded with GDP, but the interaction was markedly strengthened when loaded with GTP $_{\gamma}$ S to "lock" $G_{\alpha i2}$ in its active state (Fig. 6J).

We found that depletion of RASA2 in T cells from healthy donors enhanced TCR-induced S6-regulatory signaling pathways, cellular activation, and proliferation (Fig. 6, K and L, and fig. S20, B to D). These observations phenocopied the effects of activating $G_{\alpha i2}$ proteins and indicated that RASA2 normally negatively regulates these responses. Gene editing of P1 T cells revealed that KO of RASA2 augmented the T cell hyperactivation, consistent with the mutant $G_{\alpha i2}$ having delayed (but not completely blocked) cycling upstream of RASA2 (Fig. 6M and fig. S21).

The levels of T cell hyperactivation in RASA2 KO T cells were comparable whether or not activated $G_{\alpha i2}$ was also present (Fig. 6M and fig. S21). As the expression of the $G_{\alpha i2}$ mutant did not further activate T cells in the absence of RASA2, it indicated that activated $G_{\alpha i2}$ regulated these T cell responses completely or largely via RASA2.

These observations suggested a model in which activating $G_{\alpha i2}$ proteins, by binding RASA2, might relieve RASA2's negative regulation of S6-regulatory signaling and T cell activation. Additionally, we identified and confirmed an interaction between active $G_{\alpha i}$ 2 with PP2A Ser/Thr phosphatase complex members, PP2A-A α and PP2A-C α (Fig. 6G, fig. S20, E to I, and Data File S2). As PP2A negatively regulates both ERK/MAPK and p70S6K pathways, this interaction might reinforce the negative regulatory effects of RASA2 (35).

Thus, our data suggest that active $G_{\alpha i2}$ enhances T cell activation in a cAMP-independent manner, by preventing negative regulation by RASA2 and/or the PP2A complex.

Mutant $G_{\alpha i2}$ proteins sequestered RASA2 resulting in augmented RAS activity in T cells

Like $G_{\alpha i2}$ and other G-proteins, RAS functions according to its GDP- or GTP-bound states, and RASA2 suppresses RAS activation by accelerating RAS GTPase activity (33, 34). Patients' T cells consistently showed enhanced activation of RAS and downstream ERK1/2 upon TCR stimulation, suggesting that active $G_{\alpha i2}$ limits RASA2 activity in T cells (Fig. 7A and fig. S22, A and B). To test whether RASA2's GAP activity towards RAS was inhibited by $G_{\alpha i2}$, we mixed purified recombinant RASA2 without or with active $G_{\alpha i2}$ (loaded with GTP $_{\gamma}$ S), HRAS, and GTP, then measured RAS GTPase enzymatic activity via consumption of GTP. As GTP levels were unchanged by including active $G_{\alpha i2}$, these data suggest that $G_{\alpha i2}$ did not directly inhibit RASA2's GAP activity toward RAS (Fig. 7B, and fig. S22C).

We then considered the possibility that active $G_{\alpha i2}$ could indirectly inhibit RASA2's GAP activity by altering its cellular location. Quantitative confocal imaging in patients' cells or in cells overexpressing activating $G_{\alpha i2}$ mutants revealed that active $G_{\alpha i2}$ redistributed RASA2 toward the PM (Fig. 7, C to F, and fig. S22, D and E). By performing Förster resonance energy transfer (FRET)-based fluorescence lifetime imaging, we examined whether this membrane recruitment of RASA2 is mediated by its interaction with $G_{\alpha i2}$ (Fig. 7G). Fluorescence lifetime of a WT $G_{\alpha i2}$ -mTFP1 FRET donor was quenched only in the presence of a YFP-RASA2 acceptor, indicating that the two proteins are closely apposed (within 10 nm) (Fig. 7, G to I). Quenching was mainly observed at the cell periphery near the PM, with FRET efficiency reciprocally also increased there (fig. S22F). The mTFP1 lifetime was dramatically shorter when the activating $G_{\alpha i2}$ mutant Gln205Leu was co-expressed with RASA2 (red vs. blue color in Fig. 7H), with FRET efficiency also increased under the same conditions (fig. S22F), supporting an increased association between these two proteins.

In T cells, exogenously expressed HRAS or NRAS localizes to both the PM and Golgi, but RAS activation predominates at the Golgi during TCR activation (26, 36). Therefore, we assessed whether RAS activation at the Golgi correlates with $G_{\alpha i2}$ -mediated RASA2 redistribution to the PM after TCR stimulation. Using Jurkat cells co-expressing fluorescently-tagged RAS, active-RAS sensor (RBD), and a Golgi marker (GalT), along with $G_{\alpha i2}$ proteins, we performed confocal microscopy colocalization analysis. We observed greatly enhanced RAS activation at the Golgi when cells expressed an activating mutant $G_{\alpha i2}$ vs. normal $G_{\alpha i2}$ (intensity ratio 2–2.8, vs. 1.7) (Fig. 7, J to L, and fig. S22, G to I).

PI3K-AKT activation is PM-restricted, so the enhanced PI3K-AKT signaling in the patient T cells implied that PM RAS activity was also increased (Fig. 5, I and K; fig. S15, H and P; fig. S16, G to I; and fig. S17) (37). Because both RAS and $G_{\alpha i2}$ at the PM undergo dynamic spatiotemporal regulation, $G_{\alpha i2}$ -mediated RASA2 sequestration might also enhance local RAS activity within the PM microdomains (29, 34). Overall, our findings suggest that active $G_{\alpha i2}$ enhances TCR-induced RAS activity by physically directing RASA2 away from RAS within cells.

Discussion

Previously, activating mutations in other G_{α} subunits have been reported in various types of human cancers and diseases, and investigations have focused on their augmented downstream signaling pathways (38, 39). By studying humans with activating *GNAI2* mutations, we find enhanced suppression of effector cAMP generation and establish a pathogenic role of chronic decoupling of active $G_{\alpha i2}$ from GPCRs. Chronic decoupling can result from multiple factors such as faster GTP binding, slower intrinsic hydrolysis, and RGS insensitivity. When compounded, they could disproportionately prolong the time G-proteins take to cycle from their active free form, back to their inactive GPCR-bound form capable of responding again to GPCR agonists. Rapid G-protein cycles may be required to respond to quickly changing environmental cues, such as for optimal spatiotemporal sensing of chemokine gradients through $G_{\alpha i}$ during cell migration. A similar requirement apparently underlies rapid photoreceptor deactivation to detect sudden changes in moving objects through $G_{\alpha t}$ during spatiotemporal visual signaling (40). Nevertheless, we do not exclude a possible additional contribution of active $G_{\alpha i2}$ through sequestering or otherwise interfering with free $G_{\beta \gamma}$ signaling (21, 41–44).

While we have established that the impaired migratory behavior of immune cells leads to the patients' infection susceptibility and immune dysregulation, their additional clinical features suggest that the migratory behavior of non-immune cells is similarly impaired during development. The patients' prominent midline anatomic defects may reflect abnormal neural crest cell migration, which proceeds along the anterior-posterior axis during embryogenesis to help form many tissues (45). Such migration requires CXCL12 signaling through the CXCR4 chemokine receptor, whose deficiency causes cerebellar and other anatomical abnormalities and is embryonically lethal in mice (46). Furthermore, partial knockdown of *Gnai2* in developing mouse embryos perturbed neuronal migration during corticogenesis, consistent with $G_{\alpha,i2}$ regulating differentiated non-immune cell migration during development and paralleling defective leukocyte migration in *Gnai2* KO mice (15, 47). Unfortunately, we could not track migration of non-immune cells during development, as attempts to generate a patient-mimicking KI mouse model were unsuccessful.

Besides establishing an important physiologic requirement in vivo for the normal cycling of $G_{\alpha i2}$ during cell migration, our patients with constitutively activating mutant $G_{\alpha i2}$ reveal a $G_{\alpha i2}$ -mediated but cAMP-independent RAS-regulatory pathway that controls the amplification of T cell responses through RASA2. We now place $G_{\alpha i2}$ immediately upstream of RASA2 at the nexus of GPCR and TCR signaling pathways. In healthy individuals, this pathway could operate physiologically when $G_{\alpha i2}$ is transiently activated

by chemokine receptors, to coordinate T cell migration with and optimize TCR-induced activation and proliferation. Such a model may be consistent with the previously reported co-stimulatory contribution of chemokine receptor signaling during T cell activation (48). In patients with activating GNAI2 mutations, we propose that the resulting stronger TCR input breaks peripheral tolerance, predisposing to the autoimmunity and age-associated lymphocytosis seen in some individuals. Exploiting this $G_{\alpha i2}$ -RASA2-RAS signaling axis could facilitate development of T cell-based anti-tumor therapies. For example, improving expansion and activity of T cells expressing chimeric antigen receptor (CAR) could be achieved by fusing CAR to mutant $G_{\alpha i2}$ domains that preferentially scavenge RASA2 (49). Indeed, our observations support recent studies using CRISPR screens in primary T cells and mouse models of cancer immunotherapy that provide evidence of RASA2 as a negative regulator (50, 51). As KO of RASA2 in transgenic CD8+ T cells or CAR T cells increases antigen-specific tumor cell killing in vitro (50, 51), those results suggest that a similar approach targeting $G_{\alpha i2}$ upstream of RASA2 might also be promising.

There are several limitations to our study. First, we focused on the impact of the patients' $\mathit{GNAI2}$ mutations on their $G_{\alpha i2}$ proteins and not on $G_{\beta\gamma}$ proteins. Their activating $G_{\alpha i2}$ mutants are expected to not only decouple from GPCR but also increase dissociated $G_{\beta\gamma}$. Free $G_{\beta\gamma}$ signaling regulates chemokine-mediated cell migration by modulating phosphoinositide-3-kinase γ (PI3K γ) and possibly AC activities (52). However, one of our patients had an Arg209Trp activating mutation in the "Gly-Arg-Glu" triad, which is required for $G_{\beta\gamma}$ dissociation from G_{α} for other G-proteins (21). This variant is predicted to have the opposite effect of decreasing free $G_{\beta\gamma}$, yet it was still associated with impaired leukocyte migration. Therefore, while the activating $G_{\alpha i2}$ mutants could also exert secondary effects through increased free $G_{\beta\gamma}$, this explanation does not account for our observations. Studies addressing the impact of the activating $G_{\alpha i2}$ mutants on $G_{\beta\gamma}$ biology, including downstream spatiotemporal effects on cell polarity, adhesion, and migration, will be needed to clarify these points.

A second limitation of our study is that while we have shown that activated $G_{\alpha i2}$ acts primarily through RASA2 to drive RAS-mediated T cell hyperresponsiveness, the effect conferred by RASA2 KO was greater than by activating $G_{\alpha i2}$ alone. Several factors may account for this difference. Constitutively activating $G_{\alpha i2}$ mutants are expected to have prolonged cycling but still pass through an inactive form, which binds less well to RASA2. In our experiments, we tested Thr182Ala, but other variants having different cycling times may show different relative effect sizes. Furthermore, the relative amounts of active $G_{\alpha i2}$ vs. RASA2 in the cells and the stoichiometry required for efficient sequestration away from the Golgi are unknown. Alternatively, $G_{\alpha i2}$ -independent factors could also regulate RASA2. Additional studies are needed to address these possibilities.

Finally, based upon their activated RAS-MAPK signaling, patients with germline activating GNAI2 mutations can now be included within the RASopathy spectrum (53, 54). Indeed, our patients show clinical overlap, including autoimmunity, with patients having typical RASopathies such as Noonan syndrome (53, 55). The widespread tissue expression of $G_{\alpha i2}$ and RASA2, along with the diverse biological functions mediated by RAS proteins in cancer pathogenesis, raises the interesting possibility that the $G_{\alpha i2}$ -RASA2-RAS signaling axis

might broadly regulate growth, proliferation, and differentiation in the body. Consistent with this possibility, inhibitory roles of RASA2 in cellular growth and proliferation have been reported in fibroblast and melanoma cells (56). Additionally, somatic activating GNAI2 mutations have been identified in cancers including melanoma, adrenal cortical tumors, and ovarian sex cord stromal tumors (39, 57), paralleling loss-of-function RASA2 mutations in melanomas and dysregulated RAS activity in various human cancers (33, 34, 56, 58). Thus, our discoveries also provide fresh insight into the molecular etiology and potential therapeutic targets to disrupt $G_{\alpha i2}$ for tumors with oncogenic GNAI2 or RAS pathway mutations.

Materials and Methods

Study Participants and Human Sample Collection

The patients originated from diverse ethnicities/geographic regions (Latino/Admixed American, Non-Finnish European, European-Finnish, West Sub-Saharan African, Middle Eastern Arab). Age and sex of patients are contained in Supplementary Text 4. All enrolled subjects (patients, family members, healthy donors) provided written informed consent to participate in local Ethics or IRB-approved research protocols from various institutions (see Supplementary Materials for details). Patient or parent/legal guardian provided additional written authorization for publication of potentially identifiable facial photographs. Whole blood samples, fingernail clippings, skin punch biopsies, blister fluid, mouth washings, and skin swabs were obtained for experimental analyses in accordance with research protocols.

Mice

Animal housing, care, and experimental procedures of mice (*Mus musculus*) were performed under animal study protocols approved by the NIAID Animal Care Use Committee or the Garvan Institute of Medical Research/St Vincent's Hospital Animal Ethics Committee. Mouse euthanasia was performed by carbon dioxide inhalation followed by cervical dislocation. Wildtype (WT) B6 (C57BL/6J, strain# 000664), CD45.1 congenic B6 (B6.SJL-Ptprca Pepcb/BoyJ, strain# 002014), and Thy1.1 congenic B6 (B6.PL-Thy1a/CyJ, strain# 000406) were purchased from the Jackson Laboratory (Bar Harbor). Adoptive transfer experiments used female mice at 6 to 8 weeks of age. Generation of *Gnai2* KI embryos was as described in the Supplementary Methods.

Whole Exome Sequencing (WES), Whole Genome Sequencing (WGS), and Analyses

We conducted WES on the index patient (P1) and her healthy parents and sister. Patients 2 to 18 and 20 with mutations in the *GNAI2* gene were identified from WES or WGS data (14), either through GeneMatcher (phenotype-agnostic) or through other inquiries that were broadly immune phenotype driven (59). Exome or genome libraries from gDNA were generated, and variant calling and analysis performed using various platforms (see Supplementary Materials for details). The familial *GNAI2* mutation in P19 was identified by Sanger sequencing. In the patients, no other candidates besides *GNAI2* were shared under *de novo*, autosomal recessive (AR), or variable-penetrance autosomal dominant (AD) models of inheritance (table S1). All genomic variants in this manuscript are described according to Human Genome Variation Society recommendations (60), using GenBank

Reference Sequences NC_000003.11(gDNA), NM_002070.2 (mRNA), and NP_002061.1 (protein) based upon genome assembly Build GRCh37 unless otherwise indicated.

Characterization of Gai2 GTPase and RASA2 GAP Activities

For GTP binding and hydrolysis assays, recombinant G_{a,i2} protein was mixed with BODIPY-FL-GTP or BODIPY-FL-GTP $_{\gamma}$ S (Thermo Fisher), and the kinetics of in vitro $G_{\alpha i2}$ protein activation measured (61). To examine RGS sensitivity, $G_{\alpha i2}$ was incubated with RGS16 before adding BODIPY-FL-GTP. Nucleotide-binding data were fit with one phase exponential equation $F = a - b e^{-kt}$, where F is a specific increase of fluorescence, to obtain k. GTP binding and hydrolysis curves were fit with the equation $F = (C_0k_1 / (k_2))$ $-k_1$)) ($e^{-k_1t} - e^{-k_2t}$) for the intermediate product in two sequential reactions (62). For RGS binding assays, recombinant His6-Gai2 and GST-RGS16 were incubated together at 4 °C in the presence of a slurry of glutathione sepharose beads and either GDP or GDP plus aluminum magnesium fluoride (AMF) to mimic the transition state for GTP hydrolysis (18). Bound proteins were eluted from beads, resolved by SDS-PAGE, and immunoblotted. GAP activity of RASA2 toward RAS protein was measured according to manufacturer's instructions (Promega), with modifications. Unless stated otherwise, 1 µM His-tagged hRas (Cytoskeleton, Inc.), 0.25 μM maltose binding protein (MBP) / MBP-RASA2, and 2.5 μM GST / GST- $G_{\alpha i2}$ proteins, pre-loaded with either GDP or GTP $_{\gamma}$ S, were incubated with 5 μ M GTP and 1 mM DTT in the provided GTPase/GAP Buffer. Levels of GTP remaining were measured.

Cells, Media, and Cell Culture

Human embryonic kidney 293T cells (293T), HEK293 cell line stably lacking AC3 and AC6 (HEK-AC $\,$ 3/6) (63), Platinum-E cells, NIH/3T3, Jurkat T cells, and HL60 cells were cultured in DMEM or RPMI 1640 medium with supplements. Human peripheral blood mononuclear cells (PBMC) were isolated from whole blood by Ficoll-Paque PLUS density gradient centrifugation (Cytiva). Pan-T cells or CD4+ T cells were isolated from PBMCs by negative selection (Miltenyi Biotec), or by fluorescence-activated cell sorting (FACS) using a BD FACSAria III cell sorter. For functional studies, purified T cells were used either immediately or activated using the T Cell Activation/Expansion Kit (Miltenyi Biotec). The latter were expanded in the presence of 100 U/mL recombinant human IL-2 for 2 to 3 weeks before use. Neutrophils were isolated by density gradient separation and used immediately for experiments. Fibroblasts were isolated from skin punch biopsies and cultured as described (64). Murine leukocytes isolated from spleens, inguinal and axial lymph nodes were activated with plate bound anti-mouse CD3 (5 µg/mL) and soluble anti-mouse CD28 (1 µg/mL) and cultured in RPMI medium containing 100 U/mL recombinant human IL-2.

cAMP Measurements

293T cells (previously transfected with individual $G_{\alpha,i2}$ plasmid using polyethylenimine) or human dermal fibroblasts were stimulated at 37 °C for 20 minutes with 5 μ M forskolin (FSK) in the presence of 0.5 mM of the nonspecific inhibitor of phosphodiesterase 3-isobutyl-1-methylxanthine (IBMX). In some experiments, T cells (10 to 20 days after initial

activation) were stimulated with 50 μ M FSK/ 0.5 mM IBMX at 37 °C for 20 to 60 minutes. Cells were lysed and accumulated intracellular cAMP levels measured using the colorimetric cAMP ELISA Kit per manufacturer's instructions (Cell Biolabs). cAMP was alternatively measured using a YFP-Epac-rLuc cAMP biosensor (pcDNA3L-His-CAMYEL) in 293T cells previously transfected also with plasmids expressing $G_{\alpha i2}$ and CXCR4 (65). Cells were stimulated in BRET Buffer (0.5 mM MgCl₂ and 0.1% BSA fraction V in PBS) with FSK (0, 10^{-8} - 10^{-4} M) in the presence of 5 μ M Coelenterazine h for 10 minutes at room temperature. Luminescence and fluorescence readings were collected by sequential integration of the signals detected in the 480 ± 20 nm and 530 ± 20 nm windows for luciferase (Rluc) and YFP light emissions, respectively. Relative cAMP levels were indicated as 1/BRET (Rluc/YFP). In some experiments, 293T cells were transfected 24 hours previously with $G_{\alpha i2}$ plasmid and cAMP GloSensor reporter plasmid. Luminescence was measured at baseline and for 60 minutes after cells were treated with 2.5 μ M FSK.

Clinical Phenotyping and Analysis

Using criteria standardized across the patient cohort, clinical histories were coded into Human Phenotype Ontology (HPO) terms (66) and dysmorphology terms (defined at https://elementsofmorphology.nih.gov/index.cgi). For an individual patient, a value of "yes," "no," "ND" (not determined), or "NA" (not applicable, because of age or sex) was assigned to each HPO term (see table S4). Values were used to compute frequencies across the cohort for each HPO term. Selected midline (fig. S4A) or immune (fig. S4B) phenotypes were displayed as heatmaps, and phenotypes were also summarized at different level HPO categories.

T cell Migration Assays

Migration of T cells from patients and healthy donors 12 to 24 days post-activation, or of G_{qi2} WT- or variant- transduced healthy donor T cells, was assessed in vitro using a standard Transwell system with 5 µm membrane pore inserts. Recombinant human CXCL12 or CCL21 was added to the lower compartment with an equivalent number of CountBright Absolute Counting Beads (Thermo Fisher) to each well. After incubating at 37°C for 2 hours, the contents of the lower chamber were collected and stained with antibodies for flow cytometric analysis. The number of recovered cells was normalized to the number of CountBright Absolute Counting Beads collected. Migrated cells were expressed as % of the total number of cells collected from a well without a Transwell insert. Chemotaxis was calculated by subtracting random migration (determined by the wells without added chemokines). For in vivo assessment of T cell migration, wild-type (WT) C57BL/6 mice were purchased from the Jackson Laboratory (Bar Harbor). Mouse CD45.1*Thy1.2* and CD45.2*Thy1.2* lymphocytes were activated and transduced with retroviral particles containing MSCV-GFP-T2A-GNAI2 (WT) or MSCV-GFP-T2A-GNAI2 (WT or variants), respectively. Transduced cells (mixed 1:1) were intravenously injected into CD45.2+Thy1.1+ recipient mice, followed by anti-CD5 PE/Cy7 one hour later to label leukocytes in the splenic red pulp and the blood (67), and euthanized 3 minutes later. T cells recovered from tissues and blood were identified as donor (Thy1.2+GFP+), WT G_{ai2} transduced cells were distinguished as CD45.1⁺Thy1.2⁺GFP⁺, and variant G_{ai2} transduced cells were CD45.2+Thy1.2+GFP+. The normalized ratios of variant to WT $G_{\alpha i2}$

transduced cells were calculated by normalizing for differences in transduction efficiencies of each donor cell prep, migration differences between the non-transduced CD45.1⁺Thy1.2⁺ and CD45.2⁺Thy1.2⁺ populations, and the WT $G_{\alpha i2}$ (CD45.1⁺Thy1.2⁺) vs. WT $G_{\alpha i2}$ (CD45.2⁺Thy1.2⁺) control group mice (average of these mice was set to a ratio of 1).

Neutrophil Migration Assays

Where neutrophils could be isolated freshly from patients and tested within 24 hours, their migration to buffer or N-formylmethionine leucyl-phenylalanine (fMLP) was measured ex vivo at 37 °C using EZ-TAXIScan instrumentation (Effector Cell Institute, Tokyo, Japan) as described (68). Alternatively, $G_{\alpha i2}$ WT- or variant- transduced HL60 cells were differentiated with 1.3% DMSO for 5 days, and their migration to fMLP, CXCL12, or leukotriene B4 (LTB4) was similarly assessed. Digital images of migrating cells were captured every 15 to 30 seconds for 30 minutes to 1 hour for quantitative analysis. In some experiments, migration to fMLP of DMSO-differentiated, $G_{\alpha i2}$ -transduced HL60 cells was also evaluated using the Transwell system. In vivo migration into cutaneous blister fluid of P1 and healthy donors was evaluated 16 hours after applying a suction blister device to skin as described (69), or in the oral cavity of subjects using a timed (10 seconds) oral rinsing procedure with 10 mL of sterile saline (0.9% Sodium Chloride) (70). The cell pellets from either blister exudate or oral cavity rinses were stained with a combination of anti-human antibodies for quantitative flow cytometric analysis.

Measurement of Chemokine Receptor - Gai2 Interactions

293T cells, previously transfected with CXCR4-YFP or CCR7-YFP acceptor plasmids and $G_{\alpha i2}$ -Rluc donor plasmid, were stimulated in BRET buffer for 5 minutes at 37°C with increasing amounts of CXCL12 or CCL21 before adding 5 μ M Coelenterazine h. Luminescence and fluorescence readings were collected, and net BRET values were calculated by subtracting the background BRET signal from cells expressing only BRET donor ($G_{\alpha i2}$ -Rluc).

TCR Stimulation

Purified human T cells were stimulated in complete RPMI medium and 100 U/mL recombinant human IL-2, using 1 μ g/mL soluble anti-human CD3 (α -CD3), 1 μ g/mL soluble anti-CD3 and anti-CD28 antibodies (α -CD3/28), or beads with immobilized anti-CD2, anti-CD3, and anti-CD28 antibodies (Beads; at 1:1 bead to cell ratio; Miltenyi Biotec). In some cases, cells were previously stained with carboxyfluorescein succinimidyl ester (CFSE) or CellTrace Violet. Flow cytometry was used to analyze CD69 expression at 20 hours, or CD25 expression and CFSE dilution at 96 hours after stimulation. For transduced CD4+ T cells or Cas9/RNP transfected T cells, cells were stimulated with α -CD3/28 (0 to 1000 ng/mL), and CD69 and CD25 were examined at 18 to 20 hours later. For biochemical experiments, T cells were rested in serum-free RPMI at 37°C for one hour, incubated with 5 μ g/mL α -CD3 in serum-free RPMI containing 0.5% bovine serum albumin (BSA) on ice for 10 minutes, followed by addition of 20 μ g/mL of goat anti-mouse IgG antibodies at 37°C for 0 to 30 minutes. To stop stimulation, cells were washed with ice-cold PBS, and either lysed for immunoblot or active RAS pull-down, or fixed for flow cytometric intracellular staining.

In some experiments, inhibitors (3 μ M LY294002, 10 μ M U0126, or DMSO) were added one hour prior to, or the cAMP analog 8-CPT-cAMP 15 minutes prior to, T cell stimulation.

Gene knockout (KO) by CRISPR Cas9/RNP system

Cas9/RNP complexes were prepared according to manufacturer's instructions (IDT) (71) and transfected using a 4D nucleofector system into primary human T cells (P2 solution, program EH-100) or Jurkat T cells (SE solution, program CL-120). The total amount of transfected gRNA per nucleofection was kept constant by adding gNeg RNA as needed. CRISPR/Cas9-medited KO efficiency was evaluated by immunoblotting or estimated via TIDE assay (72). For evaluation of the patient's mutant allele-specific KO, cDNA was isolated and subjected to Sanger dideoxy sequencing. Experiments were performed 6–7 days after transfection.

GST Pull-down Assays and Mass Spectrometry Analysis

Glutathione S-transferase (GST)-fused G_{q,12} proteins bound to glutathione (GSH)-agarose resin were loaded with 500 mM GDP or GTP_vS and washed before use. For pull-down assays, MBP fusion proteins were prepared in pull-down buffer (lysis buffer with 500 μM GDP / GTP_γS and 20 mM MgCl₂), incubated with prepared GST fusion proteinbound resin, and interacting proteins were eluted for immunoblotting. Active Ras pulldown assays were performed according to manufacturer's instructions (Cytoskeleton, Inc.). For mass spectrometry analysis, clarified Jurkat T cell lysates prepared in pulldown buffer were incubated with GST- or GST-G_{a,i2}(Thr182Ala)- bound resin in the presence of GTP_{\gamma}S. Bound protein complexes were eluted and resuspended in acid extractable detergent. Samples were trypsin-digested and labeled with different isotopes using "reductive dimethylation" essentially as described for protocol C (73). Samples were mixed and a single long liquid chromatography with tandem mass spectrometry (LC-MS-MS) experiment was performed using the EASY-nLC 1000 Liquid Chromatograph interfaced with a Orbitrap FusionTM LumosTM TribridTM Mass Spectrometer (Thermo Fisher). Data were analyzed using MaxQuant (74) specifying 0 missed sites to decrease digestion difference based variation at an FDR of 1%. Mass spectrometry proteomics dataset was submitted to the ProteomeXchange Consortium via the PRIDE (75) partner repository (identifier PXD048980 and 10.6019/PXD048980).

Microscopy

Human CD4⁺ T cells or $G_{\alpha i2}$ KO Jurkat T cells transfected with plasmids expressing YFP-RASA2 and $G_{\alpha i2}$ were stained with CellBrite[®] Fix 555 plasma membrane dye (Biotium), fixed and permeabilized for endogenous RASA2 detection using polyclonal rabbit anti-RASA2 antibody (Novus Biologicals) /Alexa Fluor 488-conjugated goat anti-rabbit IgG, and DAPI-stained. RAS activation at the Golgi upon TCR stimulation was examined similarly as in (36). $G_{\alpha i2}$ KO Jurkat T cells were transfected with plasmids expressing mCherry-RBD, Cerulean-GalT, EGFP-HRAS / NRAS, and $G_{\alpha i2}$. Transfected cells were plated on non-treated or anti-CD3-coated chambered coverglasses. After 5 minutes, single cells expressing all fluorescent proteins in the field of view were imaged. Confocal images were acquired on either Airyscan-equipped LSM800 confocal (Zeiss) or SP8 confocal (Leica) microscopes. Images were taken with fixed acquisition settings, then analyzed and

automated using customized macro programs within ImageJ software. For fluorescence lifetime imaging microscopy (FLIM), 293T cells transfected with plasmids expressing mTFP1 and YFP were fixed and imaged on a Leica DMI 6000 SP5 confocal microscope. mTFP1 was excited at 805 nm with a femtosecond mode-locked (80 MHz repetition rate) Mai-Tai HP pulsed, multi-photon laser (Spectra Physics). Fluorescence was passed through a band-pass GFP filter at ET 525/50 (Chroma Technology Corp) and collected using a HPM100 Hybrid Detector R3809U-50 (Becker & Hickl; Hamamatsu Photonics). With SPC830 acquisition board, fluorescence decays were resolved by time-correlated single-photon counting. Acquired fluorescent transients were analyzed using SPCImage software according to single-life time decay and in ImageJ to determine FRET efficiencies in region of interest (ROI).

Supplementary Material

Refer to Web version on PubMed Central for supplementary material.

Authors

Hyoungjun Ham^{1,2,3,†,‡}, Huie Jing^{1,2,‡}, Ian T. Lamborn^{1,2,4,‡}, Megan M. Kober^{1,2,§}. Alexey Koval^{5,§}, Yamina A. Berchiche^{6,§}, D. Eric Anderson⁷, Kirk M. Druey⁸, Judith N. Mandl^{9,¶}, Bertrand Isidor^{10,11}, Carlos R. Ferreira¹², Alexandra F. Freeman¹³, Sundar Ganesan¹⁴, Meliha Karsak^{15,16}, Peter J. Mustillo^{17,18}, Juliana Teo¹⁹, Zarazuela Zolkipli-Cunningham^{20,21}, Nicolas Chatron^{22,23}, François Lecoquierre²⁴, Andrew J. Oler²⁵, Jana Pachlopnik Schmid^{26,27}, Douglas B. Kuhns²⁸, Xuehua Xu²⁹, Fabian Hauck³⁰, Waleed Al-Herz^{31,32}, Matias Wagner^{33,34,35}, Paulien A. Terhal³⁶, Mari Muurinen^{37,38,39}, Vincent Barlogis^{40,41}, Phillip Cruz²⁵, Jeffrey Danielson^{1,2}, Helen Stewart⁴², Petra Loid^{37,38,39}, Sebastian Rading^{15,16}, Boris Keren^{43,44}, Rolph Pfundt⁴⁵, Kol A. Zarember¹³, Katharina Vill⁴⁶, Lorraine Potocki^{47,48}, Kenneth N. Olivier⁴⁹, Gaetan Lesca^{22,23}, Laurence Faivre^{50,51}, Melanie Wong⁵², Anne Puel^{53,54,55}, Janet Chou⁵⁶, Maud Tusseau^{57,58}, Niki M. Moutsopoulos⁵⁹, Helen F. Matthews^{60,2}, Cas Simons^{61,62}, Ryan J. Taft^{63,64}, Ariane Soldatos⁶⁵, Etienne Masle-Farquhar^{66,67}, Stefania Pittaluga⁶⁸, Robert Brink^{69,70}, Danielle L. Fink²⁸, Heidi H. Kong⁷¹, Juraj Kabat¹⁴, Woo Sung Kim²⁹, Tatjana Bierhals¹⁶, Kazuyuki Meguro^{1,2}, Amy P. Hsu¹³, Jingwen Gu²⁵, Jennifer Stoddard⁷², Benito Banos-Pinero⁷³, Maria Slack^{74,#}, Giampaolo Trivellin^{75,**}, Benoît Mazel^{51,76}, Maarja Soomann²⁶, Samuel Li²⁵, Val J. Watts⁷⁷, Constantine A. Stratakis^{75,††}, Maria F. Rodriguez-Quevedo³, Ange-Line Bruel^{50,78}, Marita Lipsanen-Nyman³⁸, Paul Saultier^{40,79}, Rashmi Jain⁸⁰, Daphne Lehalle⁸¹, Daniel Torres^{1,2}, Kathleen E. Sullivan⁸², Sébastien Barbarot⁸³, Axel Neu⁸⁴, Yannis Duffourd^{50,78}, Morgan Similuk⁸⁵, Kirsty McWalter⁸⁶, Pierre Blanc⁴⁴, Stéphane Bézieau^{10,11}, Tian Jin²⁹, Raif S. Geha⁵⁶, Jean-Laurent Casanova^{53,54,55,87,88}, Outi M. Makitie^{37,38,39}, Christian Kubisch^{16,89}, Patrick Edery^{22,90}, John Christodoulou^{62,91,92}, Ronald N. Germain⁹, Christopher C. Goodnow^{66,93}, Thomas P. Sakmar^{6,94}, Daniel D. Billadeau³, Sébastien Küry^{10,11,‡‡}, Vladimir L. Katanaev^{5,95,‡‡}, Yu Zhang^{1,2,‡‡}, Michael J. Lenardo^{60,2,4}, Helen C. Su^{1,2,4,*}

Affiliations

¹Human Immunological Diseases Section, Laboratory of Clinical Immunology and Microbiology, Division of Intramural Research (DIR), NIAID, NIH; Bethesda, MD, USA.

²Clinical Genomics Program, DIR, NIAID, NIH; Bethesda, MD, USA.

³Division of Oncology Research, Schulze Center for Novel Therapeutics, Mayo Clinic; Rochester, MN, USA.

⁴Department of Pathology and Laboratory Medicine, Perelman School of Medicine, University of Pennsylvania; Philadelphia, PA, USA.

⁵Department of Cell Physiology and Metabolism, Faculty of Medicine, Translational Research Center in Oncohaematology, University of Geneva; 1211 Geneva, Switzerland.

⁶Laboratory of Chemical Biology and Signal Transduction, The Rockefeller University; New York, NY, USA.

⁷Advanced Mass Spectrometry Facility, National Institute of Diabetes and Digestive and Kidney Diseases (NIDDK), NIH; Bethesda, MD 20892, USA

⁸Lung and Vascular Inflammation Section, Laboratory of Allergic Diseases, DIR, NIAID, NIH; Bethesda, MD, USA.

⁹Lymphocyte Biology Section, Laboratory of Immune System Biology, DIR, NIAID, NIH; Bethesda, MD, USA.

¹⁰Nantes Université, CHU Nantes, Service de Génétique Médicale; F-44000 Nantes, France.

¹¹Nantes Université, CHU Nantes, CNRS, INSERM, l'institut du thorax; F-44000 Nantes, France.

¹²Skeletal Genomics Unit, Metabolic Medicine Branch, DIR, National Human Genome Research Institute (NHGRI), NIH; Bethesda, MD, USA.

¹³Laboratory of Clinical Immunology and Microbiology, DIR, NIAID, NIH; Bethesda, MD, USA.

¹⁴Biological Imaging Section, Research Technologies Branch, DIR, NIAID, NIH; Bethesda, MD 20892, USA

¹⁵Neuronal and Cellular Signal Transduction, Center for Molecular Neurobiology Hamburg (ZMNH), University Medical Center Hamburg-Eppendorf; 20246 Hamburg, Germany.

¹⁶Institute of Human Genetics, University Medical Center Hamburg-Eppendorf; 20246 Hamburg, Germany.

¹⁷Nationwide Children's Hospital; Columbus, OH, USA.

¹⁸The Ohio State University College of Medicine; Columbus, OH, USA.

¹⁹Department of Haematology, The Children's Hospital Westmead; Sydney, New South Wales, Australia.

²⁰Mitochondrial Medicine Frontier Program, Division of Human Genetics, Department of Pediatrics, Children's Hospital of Philadelphia; Philadelphia, PA, USA.

²¹Department of Pediatrics, University of Pennsylvania Perelman School of Medicine; Philadelphia, PA, USA.

²²Service de Génétique, Hospices Civils de Lyon; Lyon, France.

²³Univ Lyon, Univ Lyon 1, CNRS, INSERM, Physiopathologie et Génétique du Neurone et du Muscle, UMR5261, U1315, Institut NeuroMyoGène; 69008 Lyon, France.

²⁴Univ Rouen Normandie, Inserm U12045 and CHU Rouen, Department of Genetics and Reference Center for Developmental Disorders; FHU-G4 Génomique, F-76000, Rouen, France.

²⁵Bioinformatics and Computational Biosciences Branch, Office of Cyber Infrastructure and Computational Biology (OCICB), NIAID, NIH; Bethesda, MD, USA.

²⁶Division of Immunology, University Children's Hospital Zurich; Zurich, Switzerland.

²⁷Pediatric Immunology, University of Zurich; Zurich, Switzerland.

²⁸Neutrophil Monitoring Lab, Applied/Developmental Research Directorate, Frederick National Laboratory for Cancer Research; Frederick, MD, USA.

²⁹Chemotaxis Signal Section, Laboratory of Immunogenetics, DIR, NIAID, NIH; Rockville, MD, USA

³⁰Division of Pediatric Immunology and Rheumatology, Department of Pediatrics, Dr. von Hauner Children's Hospital, University Hospital, Ludwig-Maximilians-Universität (LMU); Munich, Germany.

³¹Department of Pediatrics, Faculty of Medicine, Kuwait University; Kuwait City, Kuwait.

³²Department of Pediatrics, Al-Sabah Hospital; Kuwait City, Kuwait.

³³Institute of Human Genetics, Technical University Munich, School of Medicine and Health; Munich, Germany.

³⁴Institute of Neurogenomics, Helmholtz Zentrum München; Neuherberg, Germany.

³⁵Department of Pediatrics, Division of Pediatric Neurology, Developmental Medicine and Social Pediatrics, University Hospital of Munich; Munich, Germany.

³⁶Division of Laboratories, Pharmacy and Biomedical Genetics, University Medical Centre Utrecht; 3584EA Utrecht, the Netherlands

³⁷Folkhälsan Research Center, Genetics Research Program; Helsinki, Finland.

³⁸Children's Hospital, University of Helsinki and Helsinki University Hospital; Helsinki, Finland.

³⁹Research Program for Clinical and Molecular Metabolism, University of Helsinki; Helsinki, Finland.

⁴⁰APHM, La Timone Children's Hospital, Department of Pediatric Hematology, Immunology, and Oncology; Marseille, France.

⁴¹Aix Marseille University, EA 3279 Research Unit; Marseille, France.

⁴²Oxford Centre for Genomic Medicine, Nuffield Orthopaedic Centre, Oxford University Hospitals, NHS Foundation Trust; Headington, Oxford OX3 7HE, UK.

⁴³Genetic Departement, Assistance Publique - Hôpitaux de Paris.Sorbonne University; Paris, France.

⁴⁴SeqOIA Laboratory, FMG2025, Paris; France.

⁴⁵Department of Human Genetics, Donders Institute for Brain, Cognition and Behaviour, Radboud University Medical Center; Nijmegen, The Netherlands.

⁴⁶LMU University Hospital I Department of Pediatrics I Division of Pediatric Neurology I MUC iSPZ Hauner - Munich University Center for Children with Medical and Developmental Complexity I Dr. von Hauner Children's Hospital; Munich, Germany.

⁴⁷Department of Molecular and Human Genetics, Baylor College of Medicine; Houston, Texas, USA.

⁴⁸Texas Children's Hospital; Houston, Texas, USA.

⁴⁹Pulmonary Branch, Division of Intramural Research, DIR, National Heart Lung and Blood Institute (NHLBI), NIH; Bethesda, MD, USA.

⁵⁰UMR1231 GAD, Inserm, Université Bourgogne-Franche Comté; Dijon, France.

⁵¹Centre de Génétique et Centre de Référence "Anomalies du Développement et Syndromes Malformatifs de l'Inter-région Est", FHU TRANSLAD, CHU Dijon Bourgogne; Dijon, France.

⁵²Department of Allergy and Immunology, The Children's Hospital at Westmead; Sydney, New South Wales, Australia.

⁵³St. Giles Laboratory of Human Genetics of Infectious Diseases, Rockefeller Branch, The Rockefeller University; New York, NY, USA.

⁵⁴Laboratory of Human Genetics of Infectious Diseases, Necker Branch, Institut National de la Santé et de la Recherche Médicale INSERM U1163; Paris, France.

⁵⁵University of Paris Cité, Imagine Institute; Paris, France.

⁵⁶Division of Immunology, Boston Children's Hospital, Department of Pediatrics, Harvard Medical School; Boston, MA, United States.

⁵⁷Genetics Department, Lyon University Hospital; Lyon, France.

⁵⁸The International Center of Research in Infectiology, Lyon University, INSERM U1111, CNRS UMR 5308, ENS, UCBL; Lyon, France.

⁵⁹Oral Immunity and Infection Section, DIR, National Institute of Dental and Craniofacial Research (NIDCR), NIH; Bethesda, MD, USA.

⁶⁰Molecular Development of the Immune System Section, Laboratory of Immune System Biology, DIR, NIAID, NIH; Bethesda, MD, USA.

⁶¹Centre for Population Genomics, Garvan Institute of Medical Research and UNSW Sydney; Sydney, NSW, Australia.

⁶²Murdoch Children's Research Institute; Melbourne, Victoria, Australia.

⁶³Institute for Molecular Bioscience, University of Queensland; St. Lucia, Queensland, Australia.

⁶⁴Illumina, Inc, San Diego; CA, USA.

⁶⁵National Institute of Neurological Disorders and Stroke (NINDS), NIH; Bethesda, MD, USA.

⁶⁶Immunogenomics Laboratory, Garvan Institute of Medical Research; Sydney, New South Wales, Australia.

⁶⁷School of Clinical Medicine, UNSW Sydney; Sydney, NSW, Australia

⁶⁸Laboratory of Pathology, Center for Cancer Research, NCI, NIH; Bethesda, MD, USA.

⁶⁹St Vincent's Clinical School, UNSW; Sydney, NSW, Australia.

 70 B cell Biology Laboratory, Garvan Institute of Medical Research; Sydney, New South Wales, Australia.

⁷¹Cutaneous Microbiome and Inflammation Section, Dermatology Branch, National Institute of Arthritis and Musculoskeletal and Skin Diseases (NIAMS), NIH; Bethesda, MD, USA.

⁷²Immunology Service, Department of Laboratory Medicine, Clinical Center, NIH; Bethesda, MD, USA.

⁷³Oxford Genetics Laboratories, Oxford University Hospitals NHS Foundation Trust; Oxford, Oxfordshire, UK.

⁷⁴Division of Allergy and Immunology, Department of Pediatrics, University of Rochester Medical Center and Golisano Children's Hospital; Rochester, NY, USA.

⁷⁵Section on Endocrinology & Genetics (SEGEN), DIR, Eunice Kennedy Shriver National Institute of Child Health and Human Development (NICHD), NIH; Bethesda, MD, USA.

⁷⁶Centre de Référence Déficiences Intellectuelles de Causes Rares, CHU Dijon Bourgogne; Dijon, France.

⁷⁷Department of Medicinal Chemistry and Molecular Pharmacology, Purdue University; West Lafayette, IN, USA.

⁷⁸Unité Fonctionnelle Innovation en Diagnostic génomique des maladies rares, FHU TRANSLAD; CHU Dijon Bourgogne, Dijon, France.

⁷⁹Aix Marseille University, INSERM; INRAe, C2VN, Marseille, France.

⁸⁰Clinical Immunology, Oxford University Hospitals NHS Foundation Trust; Oxford, OX3 9DU, UK.

⁸¹AP-HP Sorbonne Université, UF de Génétique Clinique, Centre de Référence Maladies Rares des anomalies du développement et syndromes malformatifs, Hôpital Trousseau; Paris, France

⁸²Division of Allergy and Immunology, Children's Hospital of Philadelphia; Philadelphia, PA, USA.

⁸³Nantes Université, Department of Dermatology, CHU Nantes, INRAE; UMR 1280, PhAN, F-44000 Nantes, France.

⁸⁴Department of Pediatrics, University Medical Center Hamburg-Eppendorf; 20246 Hamburg, Germany.

85Centralized Sequencing Program, DIR, NIAID, NIH; Bethesda, MD, USA.

⁸⁶GeneDx; Gaithersburg, MD, USA

⁸⁷Howard Hughes Medical Institute; New York, NY, USA.

⁸⁸Department of Pediatrics, Necker Hospital for Sick Children; Paris, France.

⁸⁹Martin Zeitz Center for Rare Diseases, University Medical Center Hamburg-Eppendorf; 20246 Hamburg, Germany.

⁹⁰Centre de Recherche en Neurosciences de Lyon, Inserm U1028, UMR CNRS 5292, Université Claude Bernard Lyon 1; Lyon, France.

⁹¹Department of Paediatrics, University of Melbourne; Melbourne, Australia.

⁹²Specialty of Child & Adolescent Health, University of Sydney; Sydney, Australia.

93Cellular Genomics Futures Institute; Sydney, NSW, Australia.

⁹⁴Karolinska Institutet, Department of Neurobiology, Care Sciences and Society, Center for Alzheimer Research, Division of Neurogeriatrics; Stockholm, Sweden.

⁹⁵Institute of Life Sciences and Biomedicine, Far Eastern Federal University; 690090 Vladivostok, Russia.

Acknowledgments

A portion of this work was previously included in I.T.L.'s Ph.D. Thesis Dissertation at the University of Pennsylvania as part of the NIH M.D./Ph.D. partnership program (76). The authors thank the patients and family members for participating in this study and making this research possible. We thank Joshua McElwee, Claudia Gonzaga-Jauregui, Julie Niemela, Minal Menezes, Alban Lermine for sequencing/bioinformatics assistance; Evan Masutani, Heardley Murdock, Michael Leney-Greene, Jing Qin, Virginie Vignard for other technical assistance;

Margaret Abaandou, Pam Angelus, Angela Wang, Tom Dimaggio, David McDermott for regulatory assistance; Priscilla Quackenbush for performing skin punch biopsies; Diane Hilligoss for suction blister induction; Jean Hammer, Corinne Happel, James Katz, Kim Keppler-Noreuil, Christopher Koh, Stacey Ardoin, Randal Olshefski, David Macdonald, Dominic Fitzgerald, Geoff Ambler, Michael Stormon, Chris Troedson, Nicole Armitage, Angela Morrow, Anahita Agharahimi, Colleen Muraresku, Veronika Baghin, Seraina Prader, Amanda Gerard, Lisa Satter, Maja Hempel, Geoffrey Weinberg for clinical care; and Godelieve Morel, Katariina Hannula-Jouppi, Juha Kere for diagnostic studies; Pam Schwartzberg, Stuart Tangye, John Kehrl, Owen Schwartz, Karen Hedin, and Virginia Shapiro for helpful discussions. Some Figures were created with BioRender.

Funding:

This work was supported by the NIH, Department of Health and Human Services, through the Intramural Research Programs of the NIAID (1ZIAAI001059 to H.C.S.; 1Z01AI000717 to M.J.L.; 1Z01AI000758 to R.N.G.; ZIAAI000939 to K.M.D.; 1ZIAAI001156 to T.J.; ZIAA1001247 to A.F.F.; 1ZICAI001244), NHGRI (1ZIAHG200407 to C.R.F), NHLBI (1ZIAHL006200 to K.N.O.), NIDCR (1ZIADE000732 to N.M.), NICHD (1ZIAHD008920 to C.A.S.), NIAMS (1ZIAAR041219 to H.H.K.), NIDDK (1ZICDK062009 to D.E.A.), and in part with federal funds from the NIAID under BCBB Support Services Contract HHSN316201300006W / 75N93022F00001 to Guidehouse, Inc. and to the NCI under Contract No. 75N91019D00024 and HHSN261200800001E. It utilized the Genomic Research Integration System (GRIS) and high-performance computational capabilities of the OCICB High Performance Computing cluster at the NIAID, Bethesda, MD. Molecular graphics and analyses were performed with UCSF Chimera, developed by the Resource for Biocomputing, Visualization, and Informatics at the University of California, San Francisco, with support from NIH P41-GM103311. H.H. was supported by a grant from the Korea Research Institute of Bioscience and Biotechnology (KRIBB) Research Initiative Program (Korean Biomedical Scientist Fellowship Program), KRIBB, Republic of Korea. I.T.L was a Medical Scientist Training Program student in the Graduate Program in Immunology at the University of Pennsylvania. Support was provided by Fonds de la Recherche en Santé du Québec, Canada (to Y.A.B.); Intramural Funding of the ZMNH (to M.K.); Japan Society for the Promotion of Science and Mochida Memorial Foundation for Medical and Pharmaceutical Research (K.M.); the French network of University Hospitals HUGO ('Hôpitaux Universitaires du Grand Ouest'), the French Ministry of Health and the Health Regional Agencies from Poitou-Charentes, Bretagne, Pays de la Loire and Centre-Val de Loire (HUGODIMS, 2013, RC14_0107) (to B.I., St.Bé.); the Swiss National Science Foundation (Project number:320030_205097) (to J.P.S.); the Foundation for Pediatric Research, Finland (to M.M.); the Howard Hughes Medical Institute, the Rockefeller University, the St. Giles Foundation, the NIH (R01AI127564), the National Center for Advancing Translational Sciences (NCATS), NIH Clinical and Translational Science Award (CTSA) program (UL1 TR001866), the French National Research Agency (ANR) under the "Investments for the Future" program (ANR-10-IAHU-01), the Integrative Biology of Emerging Infectious Diseases Laboratory of Excellence (ANR-10-LABX-62-IBEID), LTh-MSMD-CMCD (ANR-18-CE93-0008-01), the French Foundation for Medical Research (FRM) (EQU201903007798), the Square Foundation, Grandir - Fonds de solidarité pour l'enfance, the SCOR Corporate Foundation for Science, William E. Ford, General Atlantic's Chairman and Chief Executive Officer, Gabriel Caillaux, General Atlantic's Co-President, Managing Director and Head of business in EMEA, and the General Atlantic Foundation, Battersea & Bowery Advisory Group, Institut National de la Santé et de la Recherche Médicale (INSERM), and the University of Paris Cité (to A.P., J.L.C.); the Wallace Family Research Fund (to Ja.Ch.); the Care-for-Rare Foundation (C4R, 160073), the Else Kröner-Fresenius Stiftung (EKFS, 2017_A110), the German Federal Ministry of Education and Research (BMBF, 01GM2206D) (to F.H); the Hertie Foundation (P1230037 to Ma.Wa.); the National Health and Medical Research Council (APP1081858 to E.M., APP1113904 to R.B., APP1108800 to C.C.G.), the Bill and Patricia Ritchie Foundation (to E.M., C.C.G.); the Richard and Anne Borch Research Award, Purdue University (to V.J.W.); NIAID R01 AI120949, the Mayo Clinic Foundation (to D.D.B.); USPHS grant AI-139633, the Perkin Foundation (to R.S. G.); the Sigrid Jusélius Foundation, Finland (to O.M.M.); The Royal Children's Hospital Foundation through The Chair in Genomic Medicine (to Jo.Ch.); the Danica Foundation (to T.P.S.); and the Swiss National Science Foundation Grant #31003A 175658 (to V.L.K.). Research conducted at the Murdoch Children's Research Institute was supported by the Victorian Government's Operational Infrastructure Support Program. Whole exome sequencing (WES) of P1 was performed in kind by Merck. The research was made possible in part through access to data generated by the France Genomic Medicine Plan 2025. The content of this publication does not necessarily reflect the views or policies of the Department of Health and Human Services, nor does the mention of trade names, commercial products, or organizations imply endorsement by the U.S. Government.

Data and materials availability:

All data needed to evaluate the conclusions in the paper are present in the paper or the Supplementary Materials. The WES datasets, where permitted under terms of patient informed consent for patients 1 to 6, 8 to 14, and 18 were deposited to the National Center for Biotechnology Information's database of Genotypes and Phenotypes (dbGaP) (77)

(accession number phs002817.v1.p1) under controlled access for qualified investigators and their institutions in accordance with potentially sensitive patient information. WES datasets for patients P7 and P15 are available to qualified investigators through inter-institutional data transfer agreements; requests should be made through the corresponding author. WGS datasets for P17 and P20 will be deposited to the Collecteur Analyseur de Données (CAD) under controlled and secured access for CAD Scientific and Ethics Committee (CSE)-validated research projects. P13 and P14 familial mutation was deposited in the ClinVar database under accession number SCV001955127. The mass spectrometry proteomics data have been deposited to the ProteomeXchange Consortium via the PRIDE (75) partner repository with the dataset identifier PXD048980 and 10.6019/PXD048980. Patient samples are available from H.C.S. via a Materials Transfer Agreement for Human Materials from the NIH.

References and Notes

- Gilman AG, G proteins: transducers of receptor-generated signals. Annu Rev Biochem 56, 615–649 (1987). [PubMed: 3113327]
- 2. Wettschureck N, Offermanns S, Mammalian G proteins and their cell type specific functions. Physiol Rev 85, 1159–1204 (2005). [PubMed: 16183910]
- 3. Oldham WM, Hamm HE, Structural basis of function in heterotrimeric G proteins. Q Rev Biophys 39, 117–166 (2006). [PubMed: 16923326]
- 4. Syrovatkina V, Alegre KO, Dey R, Huang XY, Regulation, Signaling, and Physiological Functions of G-Proteins. J Mol Biol 428, 3850–3868 (2016). [PubMed: 27515397]
- 5. Taussig R, Iniguez-Lluhi JA, Gilman AG, Inhibition of adenylyl cyclase by Gi alpha. Science 261, 218–221 (1993). [PubMed: 8327893]
- Sunahara RK, Taussig R, Isoforms of mammalian adenylyl cyclase: multiplicities of signaling. Mol Interv 2, 168–184 (2002). [PubMed: 14993377]
- Sadana R, Dessauer CW, Physiological roles for G protein-regulated adenylyl cyclase isoforms: insights from knockout and overexpression studies. Neurosignals 17, 5–22 (2009). [PubMed: 18948702]
- 8. Solis GP et al., Pediatric Encephalopathy: Clinical, Biochemical and Cellular Insights into the Role of Gln52 of GNAO1 and GNAI1 for the Dominant Disease. Cells 10, (2021).
- Marivin A et al., Dominant-negative Galpha subunits are a mechanism of dysregulated heterotrimeric G protein signaling in human disease. Sci Signal 9, ra37 (2016). [PubMed: 27072656]
- 10. Weinstein LS, Chen M, Xie T, Liu J, Genetic diseases associated with heterotrimeric G proteins. Trends Pharmacol Sci 27, 260–266 (2006). [PubMed: 16600389]
- 11. Huang X et al., Pleiotropic phenotype of a genomic knock-in of an RGS-insensitive G184S Gnai2 allele. Mol Cell Biol 26, 6870–6879 (2006). [PubMed: 16943428]
- 12. Rudolph U et al. , Ulcerative colitis and adenocarcinoma of the colon in G alpha i2-deficient mice. Nat Genet 10, 143–150 (1995). [PubMed: 7663509]
- 13. Lyons J et al., Two G protein oncogenes in human endocrine tumors. Science 249, 655–659 (1990). [PubMed: 2116665]
- Lecoquierre F et al., Variant recurrence in neurodevelopmental disorders: the use of publicly available genomic data identifies clinically relevant pathogenic missense variants. Genet Med 21, 2504–2511 (2019). [PubMed: 31036916]
- Hamada N et al., Role of a heterotrimeric G-protein, Gi2, in the corticogenesis: possible involvement in periventricular nodular heterotopia and intellectual disability. J Neurochem 140, 82–95 (2017). [PubMed: 27787898]
- Scott EM et al., Characterization of Greater Middle Eastern genetic variation for enhanced disease gene discovery. Nat Genet 48, 1071–1076 (2016). [PubMed: 27428751]

17. Karczewski KJ et al., The mutational constraint spectrum quantified from variation in 141,456 humans. Nature 581, 434–443 (2020). [PubMed: 32461654]

- 18. S. R. Sprang, Invited review: Activation of G proteins by GTP and the mechanism of Galphacatalyzed GTP hydrolysis. Biopolymers 105, 449–462 (2016). [PubMed: 26996924]
- 19. Berman DM, Wilkie TM, Gilman AG, GAIP and RGS4 are GTPase-activating proteins for the Gi subfamily of G protein alpha subunits. Cell 86, 445–452 (1996). [PubMed: 8756726]
- 20. Lan KL et al., A point mutation in Galphao and Galphai1 blocks interaction with regulator of G protein signaling proteins. J Biol Chem 273, 12794–12797 (1998). [PubMed: 9582306]
- 21. Knight KM et al., A universal allosteric mechanism for G protein activation. Mol Cell 81, 1384–1396 e1386 (2021). [PubMed: 33636126]
- 22. Neptune ER, Bourne HR, Receptors induce chemotaxis by releasing the betagamma subunit of Gi, not by activating Gq or Gs. Proc Natl Acad Sci U S A 94, 14489–14494 (1997). [PubMed: 9405640]
- Lorenowicz MJ, Fernandez-Borja M, Hordijk PL, cAMP signaling in leukocyte transendothelial migration. Arterioscler Thromb Vasc Biol 27, 1014–1022 (2007). [PubMed: 17347487]
- 24. Hidi R et al., Phosphodiesterase and cyclic adenosine monophosphate-dependent inhibition of T-lymphocyte chemotaxis. Eur Respir J 15, 342–349 (2000). [PubMed: 10706503]
- Harvath L, Robbins JD, Russell AA, Seamon KB, cAMP and human neutrophil chemotaxis.
 Elevation of cAMP differentially affects chemotactic responsiveness. J Immunol 146, 224–232 (1991). [PubMed: 1701793]
- Jun JE, Rubio I, Roose JP, Regulation of ras exchange factors and cellular localization of ras activation by lipid messengers in T cells. Front Immunol 4, 239 (2013). [PubMed: 24027568]
- 27. Myers DR, Wheeler B, Roose JP, mTOR and other effector kinase signals that impact T cell function and activity. Immunol Rev 291, 134–153 (2019). [PubMed: 31402496]
- 28. Riller Q, Rieux-Laucat F, RASopathies: From germline mutations to somatic and multigenic diseases. Biomed J 44, 422–432 (2021). [PubMed: 34175492]
- 29. Abrahamsen H et al. , TCR- and CD28-mediated recruitment of phosphodiesterase 4 to lipid rafts potentiates TCR signaling. J Immunol 173, 4847–4858 (2004). [PubMed: 15470025]
- 30. Mosenden R, Tasken K, Cyclic AMP-mediated immune regulation--overview of mechanisms of action in T cells. Cell Signal 23, 1009–1016 (2011). [PubMed: 21130867]
- 31. Wehbi VL, Tasken K, Molecular Mechanisms for cAMP-Mediated Immunoregulation in T cells
 Role of Anchored Protein Kinase A Signaling Units. Front Immunol 7, 222 (2016). [PubMed: 27375620]
- 32. Mendoza MC, Er EE, Blenis J, The Ras-ERK and PI3K-mTOR pathways: cross-talk and compensation. Trends Biochem Sci 36, 320–328 (2011). [PubMed: 21531565]
- 33. King PD, Lubeck BA, Lapinski PE, Nonredundant functions for Ras GTPase-activating proteins in tissue homeostasis. Sci Signal 6, rel (2013). [PubMed: 23443682]
- 34. Simanshu DK, Nissley DV, McCormick F, RAS Proteins and Their Regulators in Human Disease. Cell 170, 17–33 (2017). [PubMed: 28666118]
- 35. Wlodarchak N, Xing Y, PP2A as a master regulator of the cell cycle. Crit Rev Biochem Mol Biol 51, 162–184 (2016). [PubMed: 26906453]
- 36. Bivona TG et al., Phospholipase Cgamma activates Ras on the Golgi apparatus by means of RasGRP1. Nature 424, 694–698 (2003). [PubMed: 12845332]
- 37. Manning BD, Toker A, AKT/PKB Signaling: Navigating the Network. Cell 169, 381–405 (2017). [PubMed: 28431241]
- 38. Spiegel AM, Weinstein LS, Inherited diseases involving g proteins and g protein-coupled receptors. Annu Rev Med 55, 27–39 (2004). [PubMed: 14746508]
- 39. O'Hayre M et al. , The emerging mutational landscape of G proteins and G-protein-coupled receptors in cancer. Nat Rev Cancer 13, 412–424 (2013). [PubMed: 23640210]
- 40. Nishiguchi KM et al., Defects in RGS9 or its anchor protein R9AP in patients with slow photoreceptor deactivation. Nature 427, 75–78 (2004). [PubMed: 14702087]

41. Ho MK, Yung LY, Wong YH, Disruption of receptor-mediated activation of G protein by mutating a conserved arginine residue in the switch II region of the alpha subunit. J Neurochem 73, 2101–2109 (1999). [PubMed: 10537070]

- Apanovitch DM, Iiri T, Karasawa T, Bourne HR, Dohlman HG, Second site suppressor mutations of a GTPase-deficient G-protein alpha-subunit. Selective inhibition of Gbeta gamma-mediated signaling. J Biol Chem 273, 28597–28602 (1998). [PubMed: 9786851]
- 43. Iiri T, Farfel Z, Bourne HR, Conditional activation defect of a human Gsalpha mutant. Proc Natl Acad Sci U S A 94, 5656–5661 (1997). [PubMed: 9159128]
- 44. Muntean BS et al., Galphao is a major determinant of cAMP signaling in the pathophysiology of movement disorders. Cell Rep 34, 108718 (2021). [PubMed: 33535037]
- 45. Szabo A, Mayor R, Mechanisms of Neural Crest Migration. Annu Rev Genet 52, 43–63 (2018). [PubMed: 30476447]
- Miller RJ, Banisadr G, Bhattacharyya BJ, CXCR4 signaling in the regulation of stem cell migration and development. J Neuroimmunol 198, 31–38 (2008). [PubMed: 18508132]
- 47. Kehrl JH, The impact of RGS and other G-protein regulatory proteins on Galphai-mediated signaling in immunity. Biochem Pharmacol 114, 40–52 (2016). [PubMed: 27071343]
- 48. Gollmer K et al., CCL21 mediates CD4+ T-cell costimulation via a DOCK2/Rac-dependent pathway. Blood 114, 580–588 (2009). [PubMed: 19451552]
- 49. Weinkove R, George P, Dasyam N, McLellan AD, Selecting costimulatory domains for chimeric antigen receptors: functional and clinical considerations. Clin Transl Immunology 8, e1049 (2019). [PubMed: 31110702]
- 50. Shifrut E et al., Genome-wide CRISPR Screens in Primary Human T Cells Reveal Key Regulators of Immune Function. Cell 175, 1958–1971 e1915 (2018). [PubMed: 30449619]
- 51. Carnevale J et al., RASA2 ablation in T cells boosts antigen sensitivity and long-term function. Nature 609, 174–182 (2022). [PubMed: 36002574]
- 52. Surve CR, To JY, Malik S, Kim M, Smrcka AV, Dynamic regulation of neutrophil polarity and migration by the heterotrimeric G protein subunits Galphai-GTP and Gbetagamma. Sci Signal 9, ra22 (2016). [PubMed: 26905427]
- 53. Zenker M, Clinical overview on RASopathies. Am J Med Genet C Semin Med Genet 190, 414–424 (2022). [PubMed: 36428239]
- 54. Aoki Y, Niihori T, Inoue S, Matsubara Y, Recent advances in RASopathies. J Hum Genet 61, 33–39 (2016). [PubMed: 26446362]
- Quaio CR et al., Autoimmune disease and multiple autoantibodies in 42 patients with RASopathies. Am J Med Genet A 158A, 1077–1082 (2012). [PubMed: 22488759]
- 56. Arafeh R et al., Recurrent inactivating RASA2 mutations in melanoma. Nat Genet 47, 1408–1410 (2015). [PubMed: 26502337]
- 57. Raimondi F et al., Rare, functional, somatic variants in gene families linked to cancer genes: GPCR signaling as a paradigm. Oncogene 38, 6491–6506 (2019). [PubMed: 31337866]
- 58. Krauthammer M et al., Exome sequencing identifies recurrent mutations in NF1 and RASopathy genes in sun-exposed melanomas. Nat Genet 47, 996–1002 (2015). [PubMed: 26214590]
- Sobreira N, Schiettecatte F, Valle D, Hamosh A, GeneMatcher: a matching tool for connecting investigators with an interest in the same gene. Hum Mutat 36, 928–930 (2015). [PubMed: 26220891]
- 60. den Dunnen JT et al. , HGVS Recommendations for the Description of Sequence Variants: 2016 Update. Hum Mutat 37, 564–569 (2016). [PubMed: 26931183]
- 61. Egger-Adam D, Katanaev VL, The trimeric G protein Go inflicts a double impact on axin in the Wnt/frizzled signaling pathway. Dev Dyn 239, 168–183 (2010). [PubMed: 19705439]
- 62. Lin C et al., Double suppression of the Galpha protein activity by RGS proteins. Mol Cell 53, 663–671 (2014). [PubMed: 24560274]
- 63. Soto-Velasquez M, Hayes MP, Alpsoy A, Dykhuizen EC, Watts VJ, A Novel CRISPR/Cas9-Based Cellular Model to Explore Adenylyl Cyclase and cAMP Signaling. Mol Pharmacol 94, 963–972 (2018). [PubMed: 29950405]

64. Lamborn IT et al., Recurrent rhinovirus infections in a child with inherited MDA5 deficiency. J Exp Med 214, 1949–1972 (2017). [PubMed: 28606988]

- 65. Bailes HJ, Lucas RJ, Human melanopsin forms a pigment maximally sensitive to blue light (lambdamax approximately 479 nm) supporting activation of G(q/11) and G(i/o) signalling cascades. Proc Biol Sci 280, 20122987 (2013). [PubMed: 23554393]
- 66. Gargano MA et al., The Human Phenotype Ontology in 2024: phenotypes around the world. Nucleic Acids Res 52, D1333–D1346 (2024). [PubMed: 37953324]
- 67. Anderson KG et al., Intravascular staining for discrimination of vascular and tissue leukocytes. Nat Protoc 9, 209–222 (2014). [PubMed: 24385150]
- 68. Cook SA et al., HEM1 deficiency disrupts mTORC2 and F-actin control in inherited immunodysregulatory disease. Science 369, 202–207 (2020). [PubMed: 32647003]
- 69. Kuhns DB, DeCarlo E, Hawk DM, Gallin JI, Dynamics of the cellular and humoral components of the inflammatory response elicited in skin blisters in humans. J Clin Invest 89, 1734–1740 (1992). [PubMed: 1601984]
- 70. Bender JS, Thang H, Glogauer M, Novel rinse assay for the quantification of oral neutrophils and the monitoring of chronic periodontal disease. J Periodontal Res 41, 214–220 (2006). [PubMed: 16677291]
- Seki A, Rutz S, Optimized RNP transfection for highly efficient CRISPR/Cas9-mediated gene knockout in primary T cells. J Exp Med 215, 985–997 (2018). [PubMed: 29436394]
- Brinkman EK, Chen T, Amendola M, van Steensel B, Easy quantitative assessment of genome editing by sequence trace decomposition. Nucleic Acids Res 42, e168 (2014). [PubMed: 25300484]
- 73. Boersema PJ, Raijmakers R, Lemeer S, Mohammed S, Heck AJ, Multiplex peptide stable isotope dimethyl labeling for quantitative proteomics. Nat Protoc 4, 484–494 (2009). [PubMed: 19300442]
- 74. Cox J, Mann M, MaxQuant enables high peptide identification rates, individualized p.p.b.-range mass accuracies and proteome-wide protein quantification. Nat Biotechnol 26, 1367–1372 (2008). [PubMed: 19029910]
- 75. Perez-Riverol Y et al., The PRIDE database resources in 2022: a hub for mass spectrometry-based proteomics evidences. Nucleic Acids Res 50, D543–D552 (2022). [PubMed: 34723319]
- 76. Lamborn IT et al., The Genetic, Molecular, And Cellular Bases Of Unidentified Primary Immunodeficiencies. Publicly Accessible Penn Dissertations 2016, 2410 (2016).
- 77. Mailman MD et al. , The NCBI dbGaP database of genotypes and phenotypes. Nat Genet 39, 1181–1186 (2007). [PubMed: 17898773]
- 78. Brust TF, Conley JM, Watts VJ, Galpha(i/o)-coupled receptor-mediated sensitization of adenylyl cyclase: 40 years later. Eur J Pharmacol 763, 223–232 (2015). [PubMed: 25981304]
- 79. Li H, Durbin R, Fast and accurate short read alignment with Burrows-Wheeler transform. Bioinformatics 25, 1754–1760 (2009). [PubMed: 19451168]
- 80. McKenna A et al., The Genome Analysis Toolkit: a MapReduce framework for analyzing next-generation DNA sequencing data. Genome Res 20, 1297–1303 (2010). [PubMed: 20644199]
- 81. Paila U, Chapman BA, Kirchner R, Quinlan AR, GEMINI: integrative exploration of genetic variation and genome annotations. PLoS Comput Biol 9, e1003153 (2013). [PubMed: 23874191]
- 82. Wang K, Li M, Hakonarson H, ANNOVAR: functional annotation of genetic variants from high-throughput sequencing data. Nucleic Acids Res 38, e164 (2010). [PubMed: 20601685]
- 83. Pettersen EF et al. , UCSF Chimera--a visualization system for exploratory research and analysis. J Comput Chem 25, 1605–1612 (2004). [PubMed: 15264254]
- 84. Coleman DE et al., Structures of active conformations of Gi alpha 1 and the mechanism of GTP hydrolysis. Science 265, 1405–1412 (1994). [PubMed: 8073283]
- 85. Tesmer JJ, Sunahara RK, Gilman AG, Sprang SR, Crystal structure of the catalytic domains of adenylyl cyclase in a complex with Gsalpha.GTPgammaS. Science 278, 1907–1916 (1997). [PubMed: 9417641]
- 86. Sunahara RK, Tesmer JJ, Gilman AG, Sprang SR, Crystal structure of the adenylyl cyclase activator Gsalpha. Science 278, 1943–1947 (1997). [PubMed: 9395396]

87. Bunemann M, Frank M, Lohse MJ, Gi protein activation in intact cells involves subunit rearrangement rather than dissociation. Proc Natl Acad Sci U S A 100, 16077–16082 (2003). [PubMed: 14673086]

- 88. Hanawa H et al., Efficient gene transfer into rhesus repopulating hematopoietic stem cells using a simian immunodeficiency virus-based lentiviral vector system. Blood 103, 4062–4069 (2004). [PubMed: 14976042]
- 89. Yang H, Wang H, Jaenisch R, Generating genetically modified mice using CRISPR/Cas-mediated genome engineering. Nat Protoc 9, 1956–1968 (2014). [PubMed: 25058643]
- 90. Menon S et al., Spatial control of the TSC complex integrates insulin and nutrient regulation of mTORC1 at the lysosome. Cell 156, 771–785 (2014). [PubMed: 24529379]
- 91. Dessauer CW, Tesmer JJ, Sprang SR, Gilman AG, Identification of a Gialpha binding site on type V adenylyl cyclase. J Biol Chem 273, 25831–25839 (1998). [PubMed: 9748257]
- 92. Toyama Y et al., Dynamic regulation of GDP binding to G proteins revealed by magnetic field-dependent NMR relaxation analyses. Nat Commun 8, 14523 (2017). [PubMed: 28223697]
- 93. Tang WJ, Gilman AG, Type-specific regulation of adenylyl cyclase by G protein beta gamma subunits. Science 254, 1500–1503 (1991). [PubMed: 1962211]
- 94. Li Y et al., Sites for Galpha binding on the G protein beta subunit overlap with sites for regulation of phospholipase Cbeta and adenylyl cyclase. J Biol Chem 273, 16265–16272 (1998). [PubMed: 9632686]
- 95. Feng H et al., Movement disorder in GNAO1 encephalopathy associated with gain-of-function mutations. Neurology 89, 762–770 (2017). [PubMed: 28747448]
- 96. Eccleston JL, Su H, Ling A, Heller T, Koh C, Gastrointestinal: Adult presentation of intestinal malrotation. J Gastroenterol Hepatol 31, 1382 (2016). [PubMed: 27060900]
- 97. Custer JW, Rau RE, editors, The Harriet Lane handbook: a manual for pediatric house officers. Elsevier Mosby, (2009).
- 98. Shearer WT et al., Lymphocyte subsets in healthy children from birth through 18 years of age: the Pediatric AIDS Clinical Trials Group P1009 study. J Allergy Clin Immunol 112, 973–980 (2003). [PubMed: 14610491]
- 99. Rab MAE et al., Persistent changes in circulating white blood cell populations after splenectomy. Int J Hematol 107, 157–165 (2018). [PubMed: 28952075]
- 100. Nishina H et al., Significance of Thr182 in the nucleotide-exchange and GTP-hydrolysis reactions of the alpha subunit of GTP-binding protein Gi2. J Biochem 118, 1083–1089 (1995). [PubMed: 8749330]

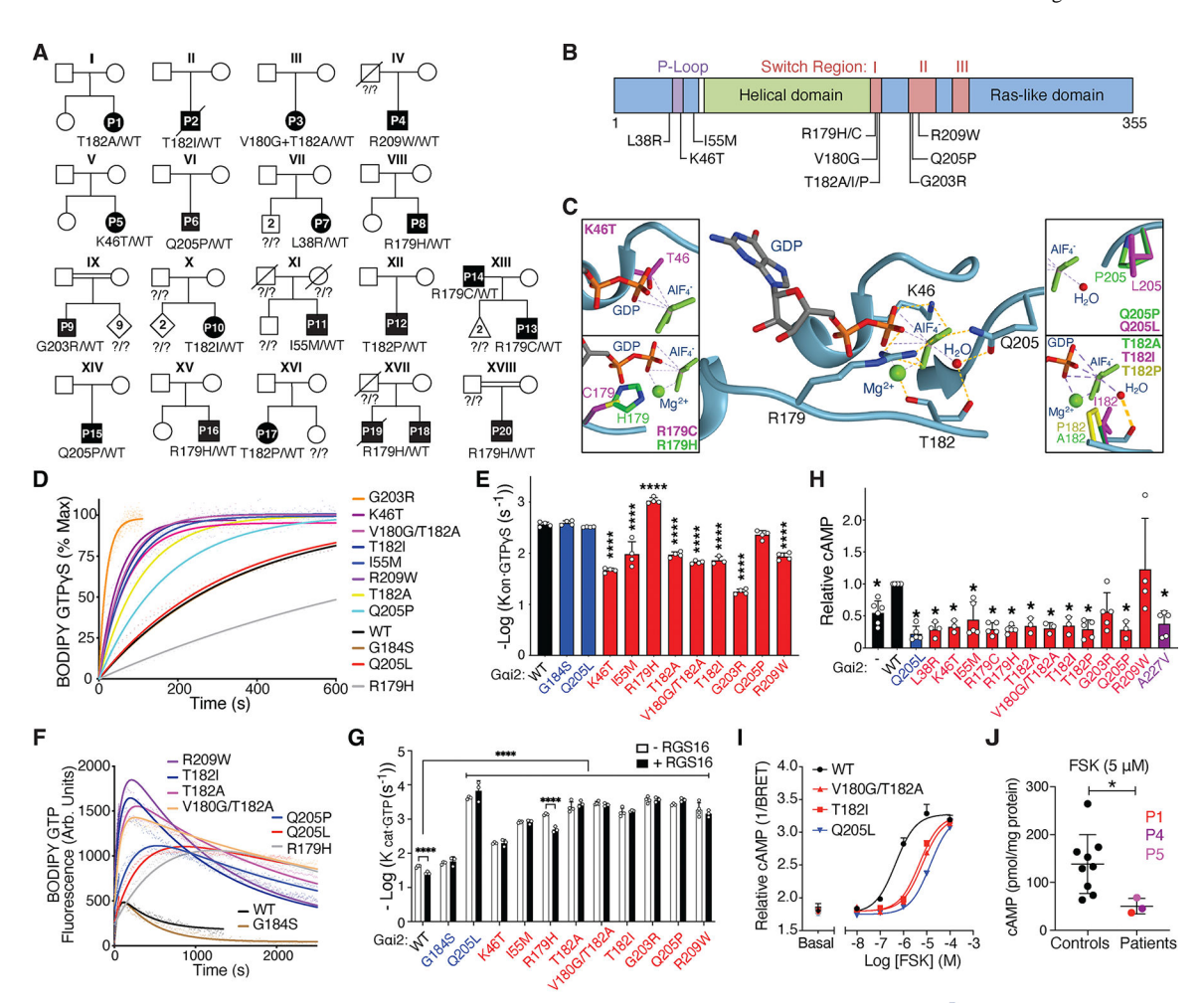


Figure 1. Humans with biochemically activating GNAI2 mutations.

(A) Patient pedigrees showing mutations and affected status. P8 was previously reported in a large cohort of individuals with developmental disorders (14). (B) Location of mutations in the Gai2 protein, numbered according to the longest isoform that predominates across tissues including blood. (C) Structural model of $G_{\alpha i2} \cdot GDP \cdot Mg^{2+} \cdot AlF4^-$ showing interactions in the GTPase catalytic site. AlF_4^- is a γ -phosphate mimic which acts as a transition state analog. Dashed lines, noncovalent bonds. Yellow, those mediated by $G_{\alpha i2}$. Insets show patient variants disrupting the interactions. The noncovalent bond between amino acid 182 and the nucleophilic H₂O is with the backbone amide oxygen on the residue. PDB: 1GFI. (**D**) GTP binding of non-hydrolyzable GTP $_{\gamma}S$ by purified recombinant $G_{\alpha i2}$ proteins. (E) Binding rate constants (k_{onGTPyS}) from (D). Red, patients' variants. Blue, Q205L, GTPase-deficient positive control (18) and G184S, RGS-insensitive control (normal GDP/GTP exchange and intrinsic GTPase activity, but impaired RGS-mediated GTPase activity) (20). (F) GTPase assay. (G) Hydrolysis rate constants (k_{catGTP}), with (black) or without (white) RGS16, from (F). (H) Forskolin (FSK)-stimulated cAMP in 293T cells after transfection with $G_{\alpha i2}$ variants, measured by ELISA. The increased cAMP in WT-transfected as compared to untransfected cells may reflect heterologous sensitization of AC (78). Purple, A227V, variant of unknown significance (15). (I) FSK-stimulated cAMP reporter activity in HEK293 cells

transfected with $G_{\alpha i2}$ variants and YFP-EPAC-RLuc reporter (and CXCR4). Relative cAMP was expressed as 1/BRET. (**J**) cAMP accumulation in primary fibroblasts from patients or healthy donors after FSK stimulation (see fig. S3I for basal levels). Data show representative (D, F, I) or mean \pm SD (E, G, H, J) for 3–5 independent experiments (D-I), or for 3 patients (J). Individual points within graphs represent results from independent experiments (E, G, H, J). Statistical analyses were performed using one-way ANOVA with Tukey's multiple comparisons for comparing individual variants to WT for (E) and (G, without RGS); multiple t-tests using the Holm-Sidak method for comparison between with or without RGS16 for each variant (G, white vs. black); one-sample t-test with Two-stage step-up method of Benjamini, Krieger and Yekutieli with hypothetical value of 1 for (H); and unpaired t-test for (J). *P<0.05; ****P<0.0001.

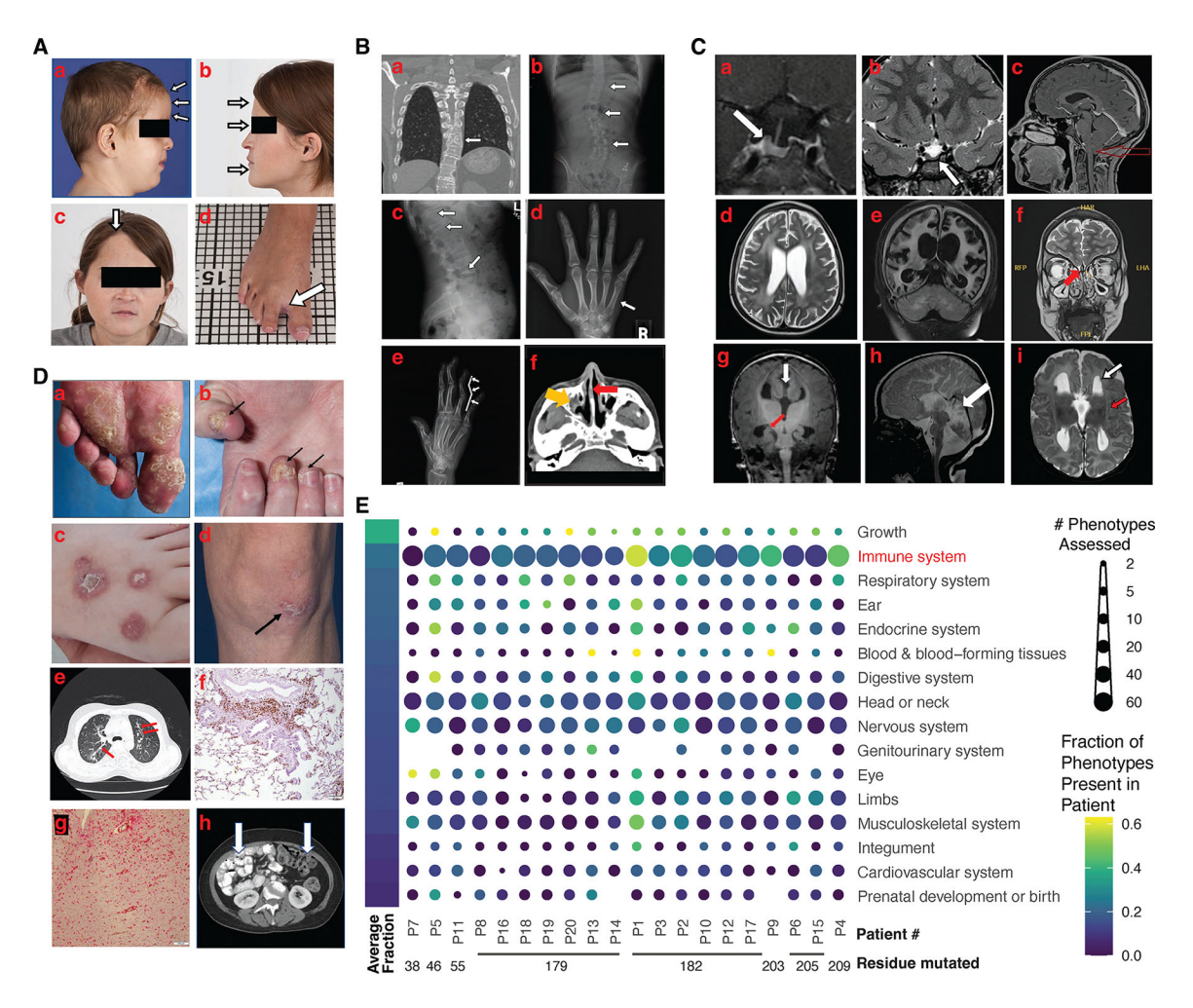


Figure 2. Selected clinical features of patients with activating GNAI2 mutations.

(A) Dysmorphism: frontal prominence (a), flat face (b), high anterior hairline (c), sandal gap deformity (d). (B) Skeletal abnormalities: sagittal cleft vertebra (a), scoliosis (b), irregular vertebral endplates (c), brachydactyly type E (d), swan-neck deformity (e), deviated nasal septum (red arrow) with chronic sinusitis (yellow arrow) (f). (C) Neurological and associated midline defects: misshapen sella turcica (a), hypoplastic pituitary gland (b), Chiari I malformation (c), diffuse leukodystrophy (d) progressing to end-stage neurodegeneration (e), absence of olfactory bulbs (arrow shown for one side) (f), agenesis of the corpus callosum (white arrow) and hippocampus malrotation (red arrow) (g), cerebellar dysplasia (h), and polymicrogyria as well as subependymal (white arrow) and band (red arrow) heterotopia (i). (D) Infectious and inflammatory complications: persistent warts (a, b), rubella-vaccine induced skin granulomas (c), psoriasiform rash (d), bronchiectasis (e), T cell infiltrates in lung (brown) (f) or brain (red) (g) in absence of infection. Intestinal malrotation (h). (E) Human phenotype ontology (HPO) summarized at top-level categories for each patient. Size of circle, number of phenotypes assessed for a patient within each category. No circle, fewer than 2 phenotypes assessed. Color scale, fraction of those phenotypes confirmed in a patient. Top-level categories were sorted from top to bottom based on the average fraction across patients. The proportion of immune phenotypes present

was tested in patients having T182 mutations ([N = 6, sample median m = 0.315, SD = 0.145] compared to those without [N = 12, m = 0.194, SD = 0.131]; t(16) = 1.788, p-value = 0.046) by a one-tailed two-sample t-test. Patients 14 and 19 were removed from this analysis since patients 13 and 14 were related and patients 18 and 19 were related.

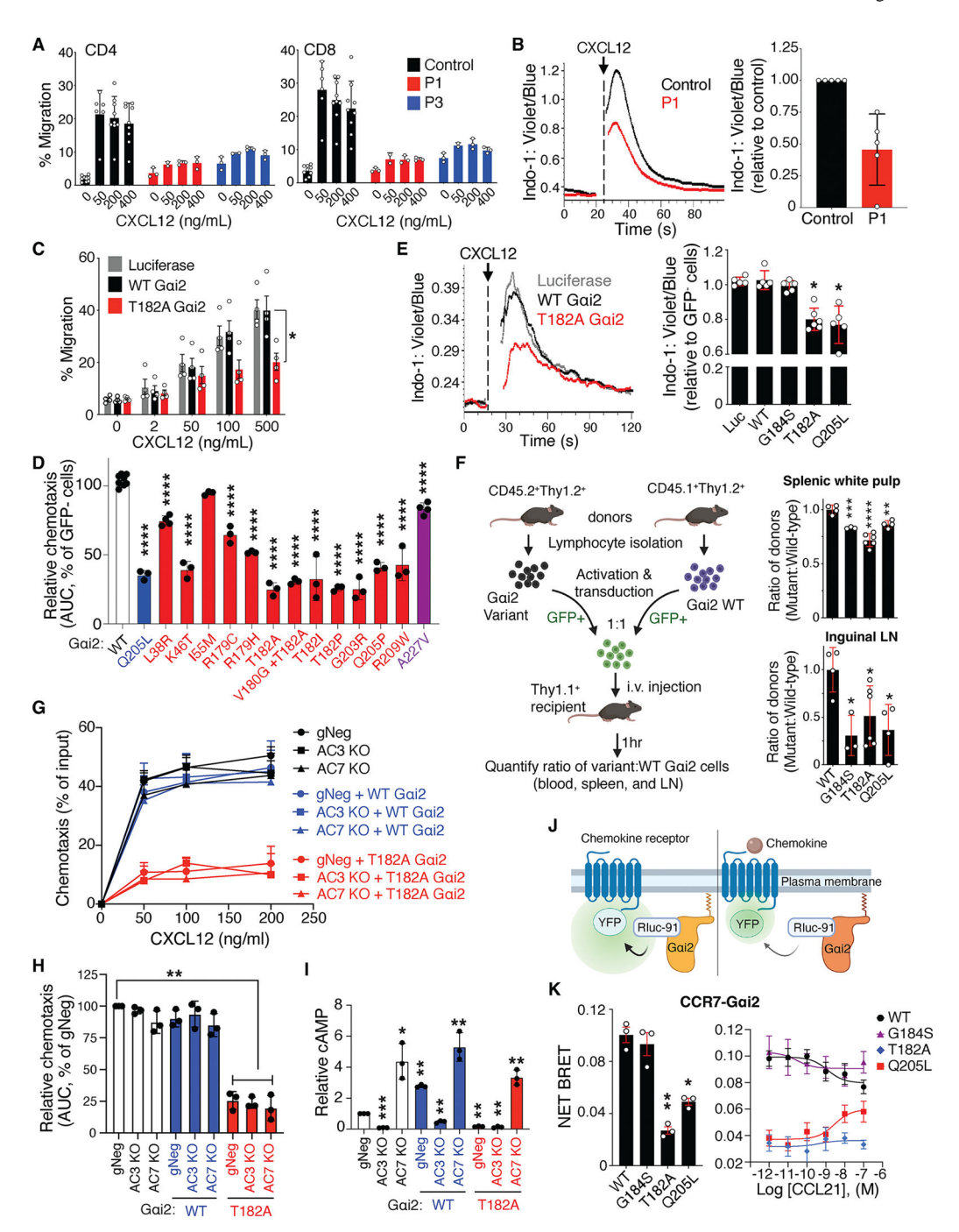


Figure 3. $G_{\alpha i2}$ mutants impair chemokine receptor signaling by decoupling from chemokine receptors.

(A) Transwell migration to chemokines of T cells from patients or healthy donors. (B) CXCL12-stimulated Ca^{2+} fluxes from a patient or healthy donor T cells (left), quantified as area under the curve (AUC) and normalized to healthy donors (right). (C) Same as (A) using healthy donor T cells stably expressing $G_{\alpha i2}$ variants or luciferase. (D) Same as (C) but quantified by normalizing AUC of transduced (GFP⁺) cells to untransduced (GFP⁻) cells. (E) Same as (B) using healthy donor T cells stably expressing $G_{\alpha i2}$ variants or

luciferase, but quantified by normalizing AUC of transduced (GFP⁺) cells to untransduced (GFP⁻) cells. (**F**) Migration after adoptive transfer of mouse T cells stably expressing G_{ai2}. Normalized ratio of variant to WT Gai2 transduced donor cells recovered from splenic white pulp or inguinal lymph node. (G) Transwell migration of AC3 or AC7 KO human T cells also stably expressing $G_{\alpha i2}$ variants or not. (H) AUC quantification of (G), normalized to gNeg-treated cells. (I) FSK-induced cAMP in cells from (G). (J) Schematized BRET reaction between Gai2-RLuc91 and GPCR-YFP. Ligand binding (right) results in a reduction of pre-ligand (left) BRET signal (green). (K) Net BRET signal between G_{a,i2}-RLuc91 and CCR7-YFP at basal conditions (left) or upon treatment with indicated chemokines (right). Gating strategies can be found in fig. S26A (for B), fig. S26B (for E), and fig. S26C (for F), and representative flow plots are presented in fig. S27A (for F). Data show representative (B, E left), means \pm SEM (C, K) or means \pm SD (A, B, E) for 3–6 (A-C, E) or 3 (K) experiments, or means \pm SD of 2 independent experiments (F, total 3–5 mice/group), or means \pm SD of 3 experiments from one of two different donor cell transductions (D, G-I). Combined results from multiple experiments are shown, with each individual point representing a different blood draw obtained longitudinally from a given patient (for A and B), or an individual recipient mouse (for F), or an independent experiment (C-E, H, I, K [left]). Statistical analyses were performed using Kruskal-Wallis test with Dunn's multiple comparisons for (C) and (E), or one-way ANOVA with Dunnett's multiple comparisons for (D), (F) and (K), or one-sample t-test with Two-stage step-up method of Benjamini, Krieger and Yekutieli for (H) and (I). *P<0.05; **P<0.01; ***P<0.001; ****P<0.0001.

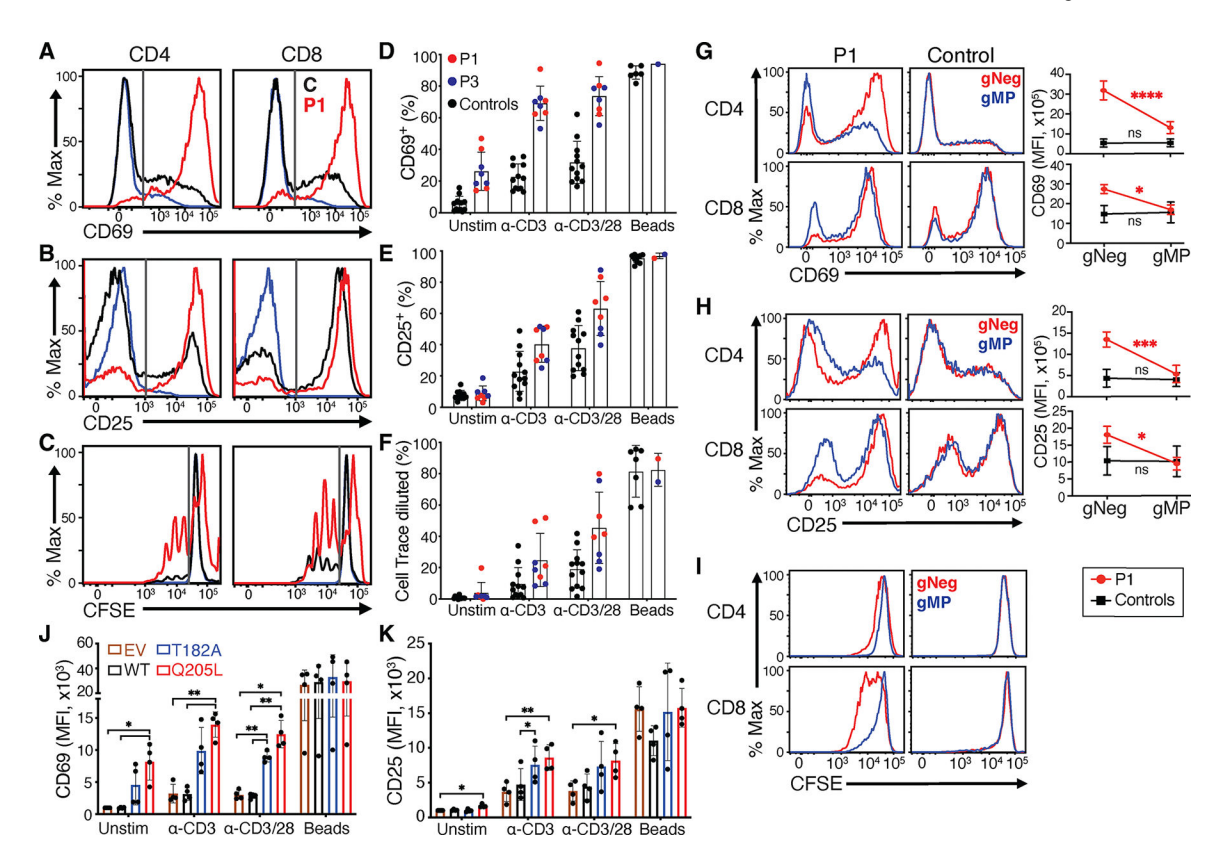


Figure 4. Activating G_{0.12} protein enhances T cell responses.

(A-F) TCR-induced surface expression of CD69 (A, D) and CD25 (B, E), and CFSE dilution (C, F) of naïve T cells purified from patient (P) or control (C) healthy donors. (A-C) Representative histograms of gated CD4⁺ (left) and CD8⁺ (right) T cells from P1 (red) and C (black) stimulated with soluble anti-CD3 and -CD28 antibodies (1 µg/mL). Unstimulated C (blue). (**D-F**) Quantification of CD69⁺ or CD25⁺ cells as % of gated CD4⁺ T cells from 2 patients and 12 controls. Each dot represents a different experiment using a different blood draw collected longitudinally over a span of 6 years. Unstim: unstimulated. α-CD3 or α-CD3/28: soluble anti-CD3 or anti-CD3 and -CD28 antibodies (1 μg/mL), Beads: bead-immobilized anti-CD2, -CD3, and -CD28 antibodies. (G-I) Same as (A-F) using P1 or control T cells treated with indicated Cas9/RNP and stimulated with anti-CD3 and anti-CD28 antibodies (0-1000 ng/mL; 100 ng/mL for representative histogram), except that Mean Fluorescence Intensity (MFI) was measured. MFI were plotted against doses of anti-CD3/28 (fig. S14D) to calculate AUC for each condition (G and H, right). gNeg is a non-specific guide RNA, and gMP targets the mutant GNAI2 allele of P1. (J and K) Same as (A, B, D, E) using CD4⁺ T cells stably expressing G_{a,i2} variants. EV: empty vector. Gating strategies can be found in fig. S26D (for A-I) and fig. S26E (for J and K). Data show representative flow plots alongside combined results with means ± SD for 4 (A-F, J and K), or 3 (G-I) experiments. Two-way ANOVA was performed with Sidak's multiple comparisons using cell type (Control or P1) and gRNA target (gNeg or gMP) as factors for (G) and (H), or one-way ANOVA with Tukey's multiple comparisons for (J) and (K). *P < 0.05; **P < 0.01; ***P < 0.001; ****P < 0.0001; ns = not significant. See also fig. S13 and S14 for related data.

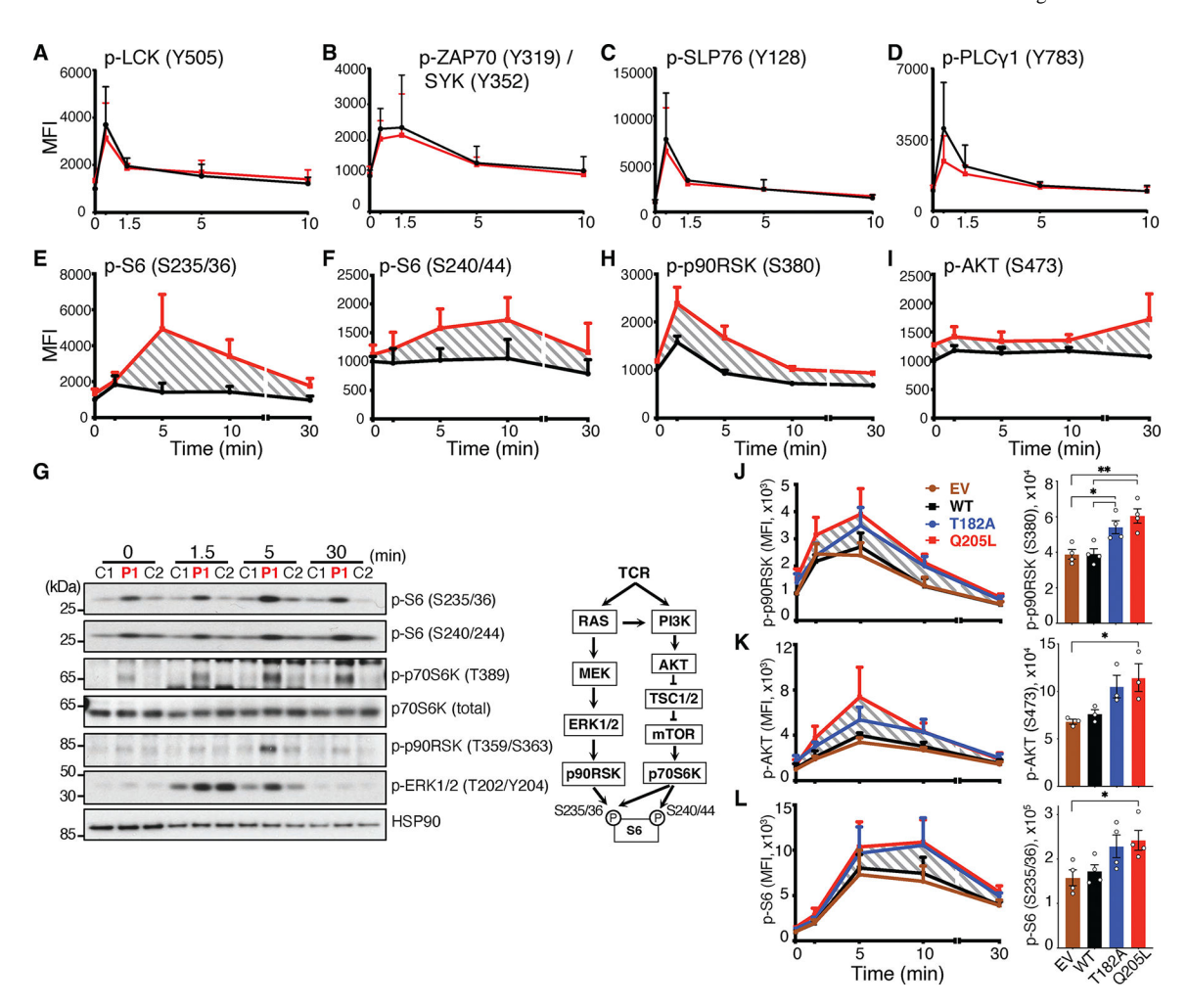


Figure 5. Active $G_{\alpha i2}$ enhances TCR-induced S6-regulatory pathways. (A-I) Purified control (C) or P1 T cells were activated with anti-CD3 antibodies for the indicated times and samples subjected to flow-cytometry or immunoblot (G, left). (A-F, H, and I) Among the gated CD4⁺ T cells, MFI was measured. (G, right) Simplified diagram of TCR-induced signaling pathways. (J-L) Similar to (A-I) using CD4⁺ T cells from a healthy donor stably expressing $G_{\alpha i2}$ variants and calculating AUC. EV: empty vector. Gating strategies can be found in fig. S26F (for A-F, H, I) and fig. S26G (for J-L). Individual data points and representative flow plots are presented in fig. S27B (for A-F, H, I) and in fig. S27C (for J-L). Data show representative (G), means \pm SEM (J-L, right), or means \pm SD (rest), based upon 3 (A-H, K), 2 (I), or 4 (rest) experiments. One-way ANOVA was performed with Dunnett's multiple comparisons for (J), (K), and (L). *P<0.05; **P<0.01.

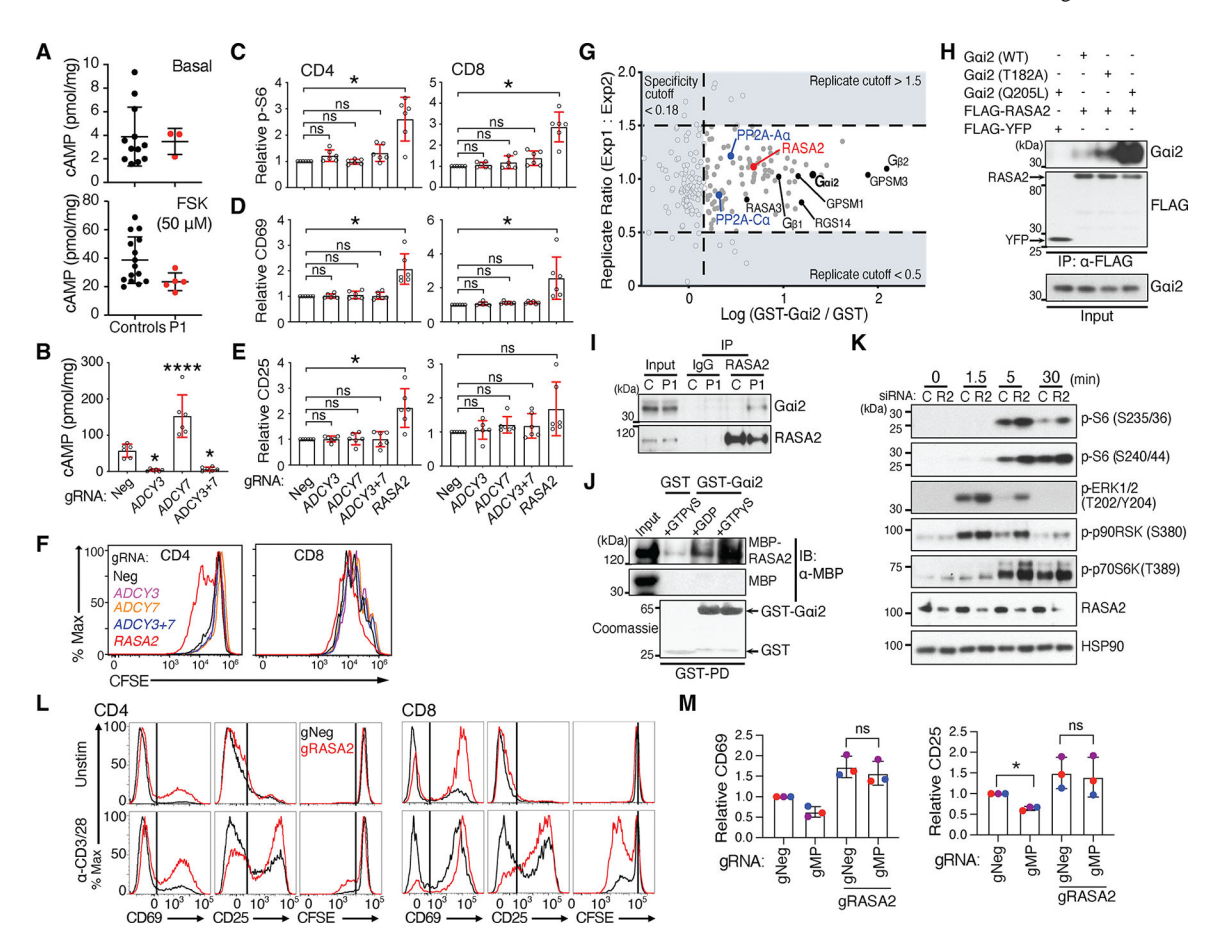


Figure 6. RASA2, a $G_{\alpha i2}$ effector target, constrains T cell responses.

(A) cAMP accumulation in control or P1 T cells at baseline (top), or upon stimulation with FSK (bottom). (B-F) T cells were transfected with indicated Cas9/RNP. (B) cAMP accumulation upon FSK treatment. (C-F) AUC quantification of TCR-induced S6 (S235/36) phosphorylation (C), surface expression of CD69 (D) or CD25 (E), and CFSE dilution (F), on gated CD4⁺ or CD8⁺ T cells, relative to gNeg control, after flow cytometric measurements of MFI. Cells were stimulated with anti-CD3 and anti-CD28 antibodies in (D and E; 0-1000 ng/mL) and in (F; 100 ng/mL). (G) Graphical representation of G_{qi2}-interacting proteins. Black: known interactors. Red and blue: candidate interactors. (H) 293T cells were transfected as indicated. FLAG was immunoprecipitated (IP) and immunoblotted (right-adjacent labels designate the specificity of antibodies used). (I) Immunoblot of RASA2 IP with T cell lysates from P1 or control (C). (J) Interaction between purified glutathione-S-transferase (GST)- $G_{\alpha i2}$ (loaded with either GDP or GTP $_{\gamma}S$) and maltose binding protein (MBP) or MBP-RASA2 fusion proteins via GST pulldown (PD). Coomassie stain: GST-fusion proteins used in PD. (K) Healthy donor T cells transfected with control (C) or RASA2-targeting (R2) siRNAs were stimulated with anti-CD3 antibodies for varying times, and lysates immunoblotted for indicated proteins. (L) TCR-induced surface expression of CD69 or CD25, and CFSE dilution of CD4⁺ or CD8⁺ T cells treated with gNeg (black) or gRASA2 (red) Cas9/RNP. Cells were stimulated with anti-CD3 and anti-CD28 antibodies (100 ng/mL). (M) AUC quantification of CD69 (left) or CD25 (right) expression on gated CD4⁺ T cells, relative to gNeg control, after flow

cytometric measurements of MFI. Purified T cells from P1 were stimulated with increasing amounts of anti-CD3 and -CD28 antibodies (0-1000 ng/mL) after transfecting with the indicated Cas9/RNP9s (gNeg, gMP targeting mutant GNAI2 allele of P1, gRASA2). Each colored dot indicates an experiment from a different blood draw. Gating strategies can be found in fig. S26F (for C), fig. S26D (for D-F), fig. S26H (for L and M). Representative flow plots are presented in fig. S27D (for C), fig. S27E (for D), fig. S27F (for E), and fig. S27P (for M). Combined results from multiple experiments are shown with each individual point representing an independent experiment (A-E, M). Data show representative (F, H-L) or means \pm SD (rest), based upon 3 (A [top], H-K, M), 5 (L), 5 (A [bottom]), or 6 (B-F) experiments. (G) shows the analysis combined from two independent PD experiments. Oneway ANOVA was performed with Dunnett's multiple comparisons for (B); one-sample t-test with Two-stage step-up method of Benjamini, Krieger and Yekutieli correction for multiple comparisons was performed with hypothetical value of 1 for (C-E); one-way ANOVA with Sidak's multiple comparisons was performed to compare gNeg vs. gMP, gNeg vs. gRASA2, gNeg vs. gRASA2+gMP, or gRASA2 vs. gRASA2+gMP in (M). *P<0.05; ****P<0.0001; ns (not significant).

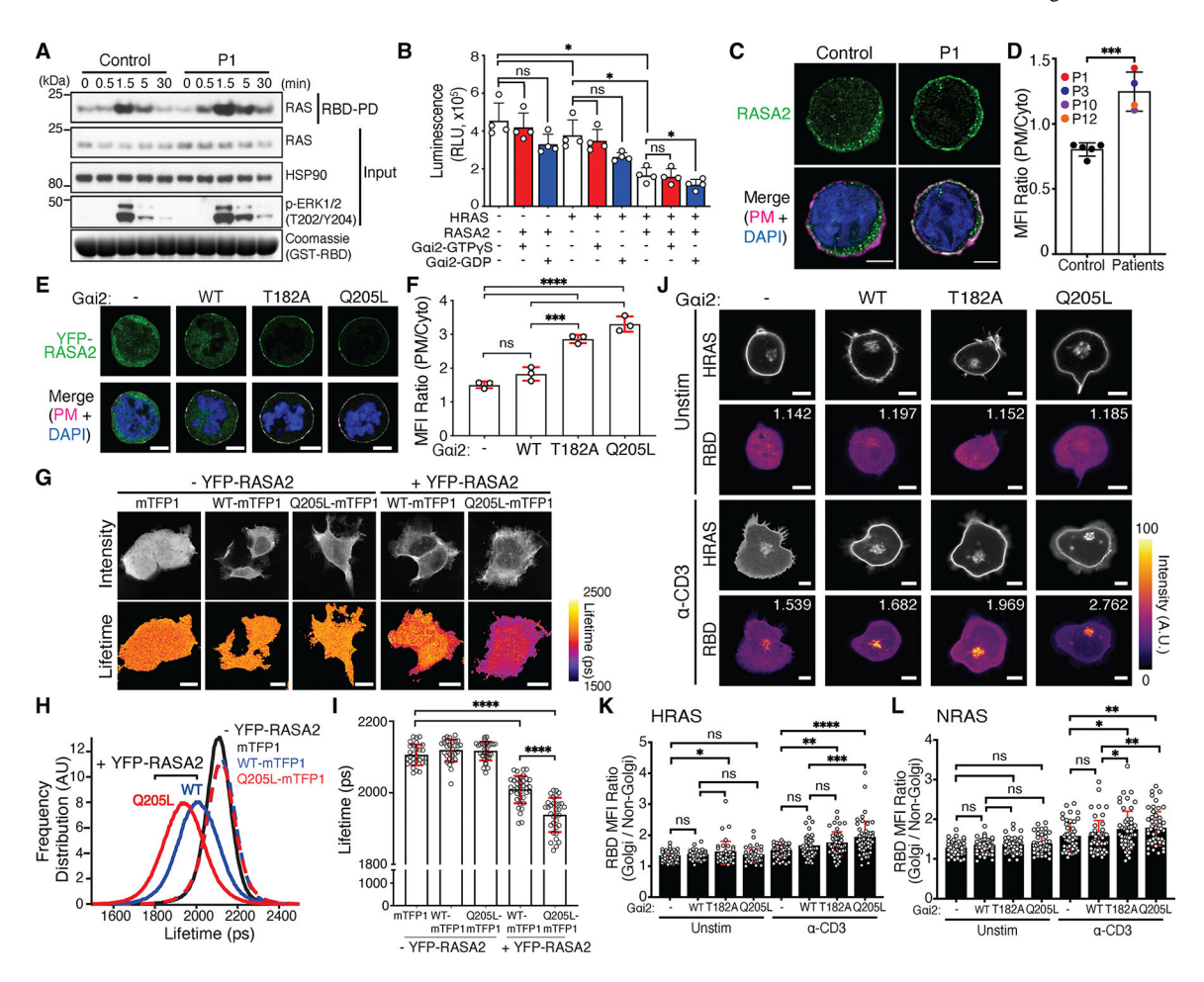


Figure 7. Active Gai2 promotes RAS activity by redirecting RASA2 to plasma membrane. (A) Control or P1 T cells were stimulated with anti-CD3 antibodies for varying times. Lysates were prepared for RBD pull down (PD) to detect active-RAS or for immunoblot for indicated proteins. Coomassie staining shows GST-RBD used in PD. (B) Purified HRAS, RASA2, and $G_{\alpha i2}$ proteins (preloaded with $GTP_{\gamma}S$ [non-hydrolyzable GTP analog that locks $G_{\alpha i2}$ in active state] or GDP) were incubated as indicated with an excess of GTP. GTP consumption was determined by measuring remaining GTP level (represented by relative light units [RLU]). (C) RASA2 distribution in CD4⁺ T cells from P1 or healthy donor control. PM: plasma membrane. (D) MFI of RASA2 ratio, at the PM relative to cytoplasm region (Cyto) in (C) and fig. S22D from 4 patients and 5 controls. (E) Distribution of YFP-RASA2 in $G_{\alpha i2}$ KO Jurkats co-expressing indicated $G_{\alpha i2}$ variants. (F) Quantification of (E) as done in (D). (G-I) Fluorescence lifetime imaging (FLIM) of mTFP1 or G_{a.i2}-mTFP1 (WT, Q205L) with or without YFP-RASA2 expression in 293T cells. (G) Fluorescence intensity (top), and lifetime (bottom) of mTFP1. (H) mTFP1 Fluorescence lifetime distribution. (I) Quantification of mTFP1 mean fluorescence lifetime. (J-L) Confocal microscopy colocalization analysis of unstimulated or TCR-induced active RAS distribution in Gai2 KO Jurkats transfected with EGFP-HRAS (J and K) or NRAS (L), mCherry-RBD, and Cerulean-GalT along with $G_{\alpha i2}$ variants as indicated. Unstim: unstimulated. (J) Number on RBD image represents MFI ratio of RBD at Golgi (defined

by GalT stain) relative to non-Golgi region. (**K** and **L**) Quantification of RBD MFI ratio as in (J). Scale bar = $3 \mu m$ (C), $5 \mu m$ (E, J) or $10 \mu m$ (G). Data show representative or means \pm SD for 3 (A, C-I, L) or 4 (B, J, K) experiments. Combined results from multiple experiments are shown (for B, D, and F), with each individual point representing an independent experiment (or a different patient for D). Each individual circle (for I, K, and L) corresponds to the value from a different cell, but with superimposed means \pm SD from across multiple independent experiments. One-way ANOVA was performed with Tukey's multiple comparisons for (B) and (F); unpaired t-test for (D); two-way ANOVA was performed using mutant type and experiment as factors for (I); three-way ANOVA was performed using transfectant, stimulation, and experimental repeat as factors for (K) and (L) and Tukey multiple comparison conditional on the stimulation status. *P<0.05; **P<0.01; ***P<0.001; ***